SANDSTONE PETROGRAPHY OF CONTINENTAL DEPOSITIONAL SEQUENCES OF AN INTRAPLATE RIFT BASIN: WESTERN CAMEROS BASIN (NORTH SPAIN)

JOSÉ ARRIBAS,[1] ÁNGELA ALONSO,[2] RAMÓN MAS,[3] AMPARO TORTOSA,[1] MAGDALENA RODAS,[4] JOSÉ F. BARRENECHEA,[4] JACINTO ALONSO-AZCÁRATE,[5] AND ROSANA ARTIGAS[4]

[1] *Departamento de Petrología y Geoquímica, Facultad de Ciencias Geológicas, Universidad Complutense de Madrid, 28040-Madrid, Spain*
e-mail: arribas@geo.ucm.es

[2] *Laboratorio de Geología, Universidad de A Coruña, Spain*

[3] *Departamento de Estratigrafía, Facultad de Ciencias Geológicas, Universidad Complutense de Madrid, 28040-Madrid, Spain*

[4] *Departamento de Cristalografía y Mineralogía, Facultad de Ciencias Geológicas, Universidad Complutense de Madrid, 28040-Madrid, Spain*

[5] *Departamento de Física-Química, Facultad de Ciencias del Medio Ambiente, Universidad de Castilla–La Mancha, 45004-Toledo, Spain*

ABSTRACT: **The Cameros Basin in Central Spain is an intraplate rift basin that developed from Late Jurassic to Middle Albian time along NW–SE trending troughs. The sedimentary basin fill was deposited predominantly in continental environments and comprises several depositional sequences. These sequences consist of fluvial sandstones that commonly pass upward into lacustrine deposits at the top, producing considerable repetition of facies. This study focused on the western sector of the basin, where a total of seven depositional sequences (DS-1 to DS-7) have been identified.**

The composition of sandstones permits the characterization of each sequence in terms of both clastic constituents and provenance. In addition, four main petrofacies are identified. Petrofacies A is quartzosedimentolithic (mean of $Qm_{85}F_2Lt_{13}$) and records erosion of marine Jurassic pre-rift cover during deposition of fluvial deposits of DS-1 (Brezales Formation). Petrofacies B is quartzofeldspathic (mean of $Qm_{81}F_{14}Lt_5$) with $P/F > 1$ at the base. This petrofacies was derived from the erosion of low- to medium-grade metamorphic terranes of the West Asturian–Leonese Zone of the Hesperian Massif during deposition of DS-2 (Jaramillo Formation) and DS-3 (Salcedal Formation). Quartzose sandstones characterize the top of DS-3 (mean of $Qm_{92}F_4Lt_4$). Petrofacies C is quartzarenitic (mean of $Qm_{95}F_3Lt_2$) with $P/F > 1$ and was produced by recycling of sedimentary cover (Triassic arkoses and carbonate rocks) in the SW part of the basin (DS-4, Peñacoba Formation). Finally, depositional sequences 5, 6, and 7 (Pinilla de los Moros–Hortigüela, Pantano, and Abejar–Castrillo de la Reina formations, respectively) contain petrofacies D. This petrofacies is quartzofeldspathic with P/F near zero and a very low concentration of metamorphic rock fragments (from $Qm_{86}F_{11}Lt_4$ in Pantano Formation to $Qm_{73}F_{26}Lt_1$ in Castrillo de la Reina Formation). Petrofacies D was generated by erosion of coarse crystalline plutonics located in the Central Iberian Zone of the Hesperian Massif. In addition to sandstone petrography, these provenance interpretations are supported by clay mineralogy of interbedded shales. Thus, shales related to petrofacies A and C have a variegated composition (illite, kaolinite, and randomly interlayered illite-smectite mixed-layer clays); the presence of chlorite characterizes interbedded shales from petrofacies B; and Illite and kaolinite are the dominant clays associated with petrofacies D.

These petrofacies are consistent with the depositional sequences and their hierarchy. An early megacycle, consisting of petrofacies A and B (DS-1 to DS-3) was deposited during the initial stage of rifting, when troughs developed in the West Asturian–Leonese Zone. A second stage of rifting resulted in propagation of trough-bounding faults to the SW, involving the Central Iberian Zone as a source terrane and producing a second megacycle consisting of petrofacies C and D (DS-4, DS-5, DS-6, and DS-7). Sandstone composition has proven to be a powerful tool in basin analysis and related tectonic inferences on intraplate rift basins because of the close correlation that exists between depositional sequences and petrofacies.

INTRODUCTION

The Cameros Basin, located in the northern part of the Iberian Range, is one of the basins forming part of the Mesozoic Iberian Rift System (Mas et al. 1993; Guimerà et al. 1995; Salas et al. 2001). The Iberian Rift System was inverted during the Paleogene and today corresponds to the Iberian Range (Fig. 1). The Cameros Basin was formed during intraplate rifting which took place from Late Jurassic to the Early Albian time, when Iberia was separated from Europe, in conjunction with the opening of the oceanic Bay of Biscay Basin. At this time several basins were formed along the NW–SE trending Iberian trough. The Cameros Basin is the most northwestern basin in the Mesozoic Iberian Rift System (Salas et al. 2001). This inboard position resulted from a minor marine influence and a delaying of the processes of diastrophism, because the rifting started first in the southeastern part of the trough and then propagated towards the northwest (Salas et al. 2001). However, in spite of its interior position, the Cameros Basin experienced the most subsidence of any basin in the Iberian Rift System, accumulating a thick pile of clastic sediments (up to 9000 m in the depocenter area). These sediments were derived from erosion of the Hercynian basement (metamorphic and crystalline rocks) and the Mesozoic sedimentary cover (Triassic and Jurassic). This sedimentary infill comprises several sequences consisting mainly of fluvial sandstones and lesser amounts of conglomerates that commonly pass upward into lacustrine carbonates and marls at the top of each sequence. The repetition of facies makes differentiation of the clastic units difficult, especially so because biostratigraphic data are scarce.

Sandstone petrography is widely considered to be a powerful tool for determining the origin and tectonic reconstructions of ancient terrigenous deposits (e.g., Blatt 1967; Dickinson 1970; Pettijohn et al. 1972). Variations in clay-mineral assemblages within shaly and marly beds also may be useful for detecting changes in the source areas in sedimentologically homogeneous materials (Alonso-Azcárate et al. 1997). Sandstone and clay mineralogical characterization of basin fill is critical to any basin analysis, and many studies have pointed to an intimate relationship between detrital sand composition (i.e., bedrock composition of the sources) and tectonic setting (e.g., Ingersoll 1978; Dickinson and Suczek 1979; Dickinson et al. 1983; Dickinson 1985; Valloni 1985; Schwab 1986; DeCelles and Hertel 1989; Critelli 1999). Sand composition also is sensitive to a complex set of factors involved in the clastic sediment system (climate, relief, transport, diagenesis), which provides valuable information for paleogeologic reconstructions (e.g., Johnsson 1993). The clay-mineral assemblage also is affected by such factors, although data must be regarded cautiously because postdepositional processes may produce significant variations from original compositions. Therefore, sand composition can supplement in sequence stratigraphic analysis in deciphering stratigraphic boundary surfaces and the internal anatomy of unconformity-bounded units of basin fill (Fontana et al. 1989; Zuffa et al. 1995).

The purpose of this study was to analyze the sandstone composition and clay-mineral assemblages of the sedimentary infill in the western sector of the Cameros Basin. These data throw light on the evolution of source areas

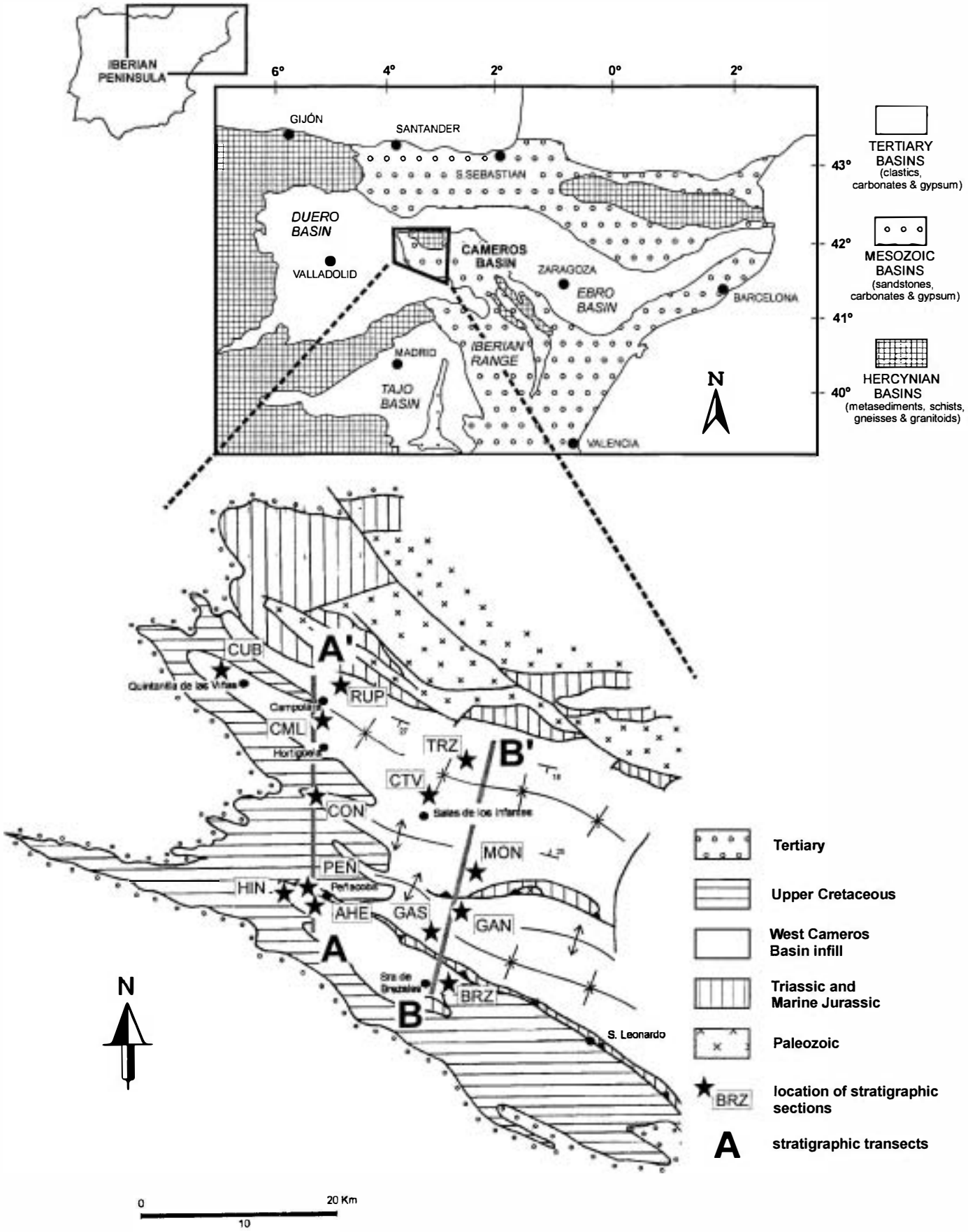

FIG. 1.—Simplified geologic map showing study area and location of stratigraphic transects A and B. These transects are shown in Figures 3 and 4, respectively.

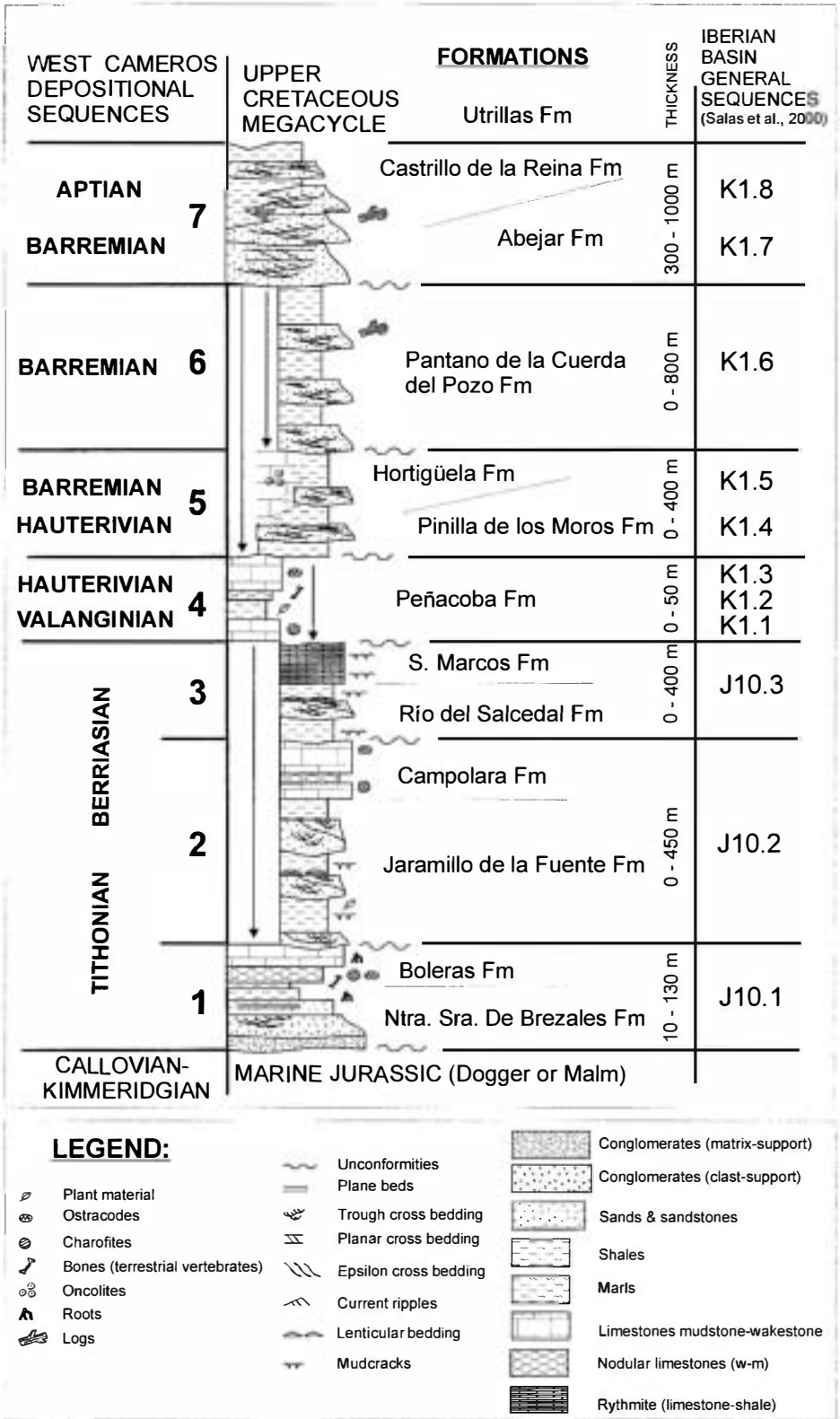

FIG. 2.—Uppermost Jurassic to Lower Cretaceous stratigraphic units and depositional sequences for western Cameros Basin, modified from Martín-Closas and Alonso Millán (1998), and correlation with general sequences from the Iberian Basin.

during the main rifting events. In addition, they allow a test of the model of depositional sequences developed by Mas et al. (1993) and Guimerà et al. (1995).

Relatively few studies have investigated the relationship between petrofacies and depositional sequences. These studies have been carried out mainly on deep-marine successions, where sea-level changes and intrabasinal sources of sediment exert a decisive influence on detrital composition (e.g., Zuffa et al. 1995). However, little is known about the relationship between composition of sediments and depositional sequences in a continental setting. In continental rift basins, tectonisms exert the main control

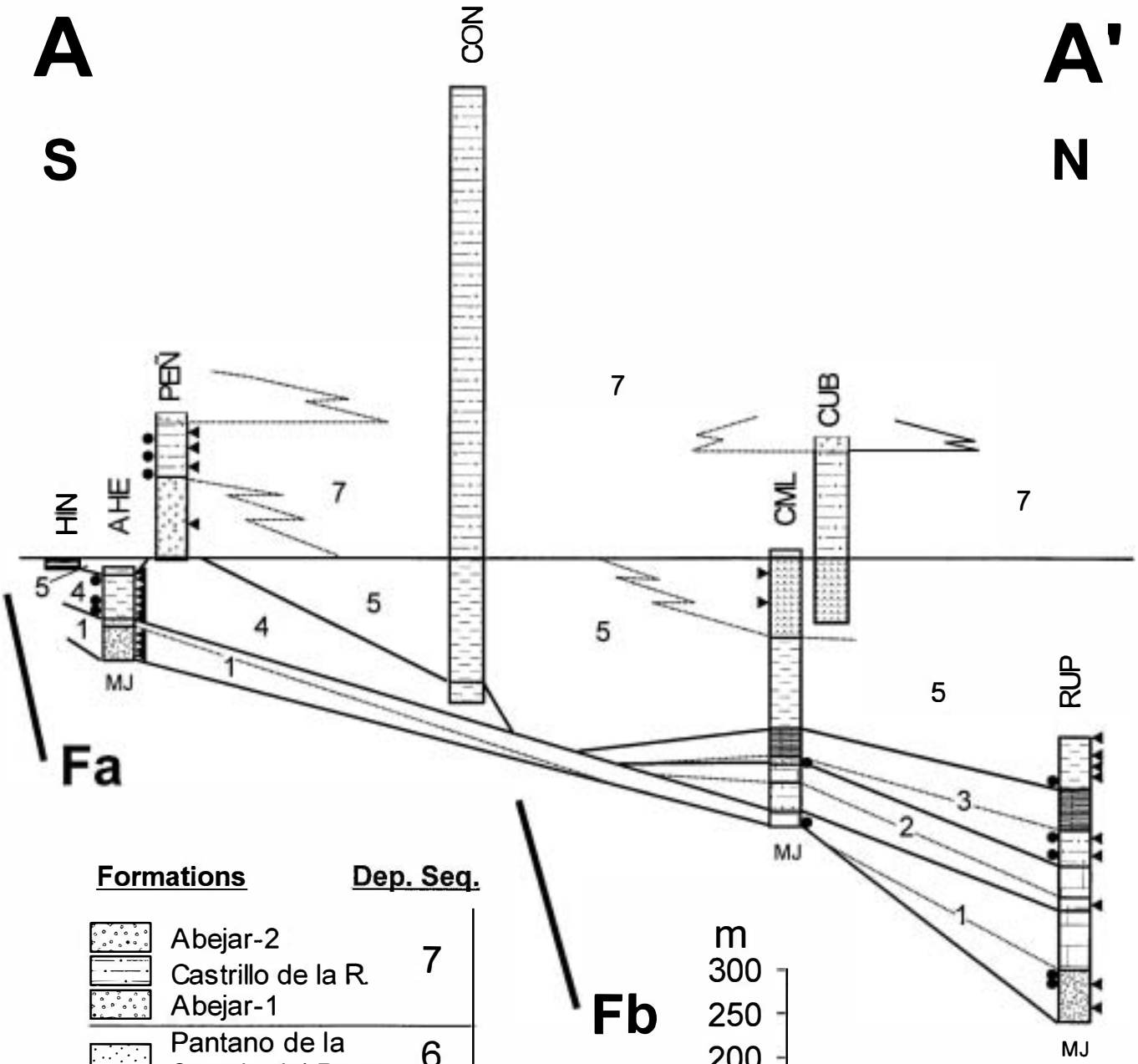

Formations	Dep. Seq.
Abejar-2 Castrillo de la R. Abejar-1	7
Pantano de la Cuerda del Pozo	6
Hortigüela Pinilla de los M.	5
Peñacoba	4
S. Marcos Salcedal	3
Campolara Jaramillo	2
Boleras Brezales	1

MJ Marine Jurassic

m
300
250
200
150
100
50
0
0 1 2 km

▸ sandstones
• shales

Location of samples

on topography and drainage-basin development (Prosser 1993). Tectonics also determines the sediment flux from catchments, which is modulated by the lithology at the source (Palomares and Arribas 1993) and by the climate (Leeder 1995). Obviously, these factors strongly control the composition of sediments (Johnsson 1993). Thus, this study is an opportunity to analyze the balance between the source-rock signal and the environmental signal (climate, transport, etc.) on sediment composition during the generation of depositional sequences in an intraplate rift basin. Finally, this paper documents sandstone composition and its evolution in a well known intraplate rift (Mas et al. 1993), and may contribute to a better understanding of sandstone modes in other equivalent geotectonic settings (e.g., Hiscott et al. 1990; Ziegler et al. 2001; Wilson et al. 2001).

GEOLOGICAL SETTING AND STRATIGRAPHY

The Cameros Basin has been interpreted as an extensional rift basin that formed above a south-dipping ramp on a blind, low-angle normal fault several kilometers deep in the basement (Mas et al. 1993; Guimerà et al. 1995; Salas et al. 2001). Two sectors can be distinguished: (1) the eastern sector, where fill is the thickest and where metamorphism appears; and (2) the western sector, where important variations in sediment thickness exist because of the complex structure of the basin. The lack of metamorphism and the existence of secondary depocenters in the western sector have been related to the movement and rotation of isolated blocks. In this sector, sedimentation took place along NW–SE trending troughs with different subsidence rates and several episodes of reactivation.

The response to Tertiary tectonic inversion was different in the two sectors. In the eastern sector a new E–W trending thrust to the north was formed, with a maximum displacement of 28 km (Guimerà et al. 1995) and with very little surface deformation. In the western part, relatively intense deformation is reflected in a system of imbricate thrusts and southward-propagating folds, reflecting a shortening of 3 km (Guimerà et al. 1995).

The area of this study is located in the northern part of the western Cameros Basin (Fig. 1). A SSW–NNE trending geological cross section of this area is shown in figure 4 (C–C′ cross section) of Guimerà et al. (1995). In this area, Martín-Closas and Alonso Millán (1998) described seven depositional sequences (DS) ranging in age from Tithonian to Aptian (Fig. 2).

Depositional Sequence 1 (DS-1) is present across the basin. Its base is defined by a major unconformity manifested as an exposed, fractured, karst surface on Callovian–Kimmeridgian limestone and sandstone. This sequence contains two lithostratigraphic units represented by alluvial and lacustrine facies. The basal unit (Nuestra Señora de Brezales Formation) is 10 to 70 m thick and consists mainly of red silty clays and polymictic conglomerates that were deposited in paleochannels of alluvial fans that pass laterally and upwards to lacustrine facies (Boleras Formation) with well-developed hydromorphic paleosols. The lacustrine facies are 60 m thick and represent the distal facies of the alluvial system. Depositional Sequence 2 (DS-2) consists of a basal fluvial unit, consisting of lenticular sandstone bodies, silty clays, and minor thin interbedded limestones (Jaramillo de la Fuente Formation) up to 400 m thick, which grade upward and laterally into lacustrine facies (Campolara Formation), nearly 100 m thick. The Campolara Formation commonly displays palaeosol levels, and the fossil content includes charophites, ostracodes, and gastropods. Depositional Sequence 3 (DS-3) comprises a basal unit deposited in a meandering fluvial system (Río del Salcedal Formation) up to 400 m thick, that grades up into lacustrine limestones and marls (San Marcos Formation), containing ostracodes, a few charophites, and abundant stromatolitic layers. Dinosaur prints are relatively common towards the top of the unit. This depositional sequence appears only in the northern part of the study area, as does DS-2. Depositional Sequences 1 to 3 can be viewed as a megacycle whose age ranges from Tithonian to Berriasian (Fig. 2). Depositional Sequence 4 (DS-4) consists of a series of limestones, lenticular sandstone bodies, marls, and clays with abundant charophytes, ostracodes, and fragments of dinosaur bones (Peñacoba Formation) up to 50 m in thickness. This sequence is spatially restricted to the south of the study area (sections HIN, AHE, PEÑ in Fig. 3 and GAS in Fig. 4). The age is Valanginian–Hauterivian (Fig. 2). Depositional Sequence 5 (DS-5) in western Cameros consists mainly of the Pinilla de los Moros and Hortigüela formations. The first unit consists of channelized fluvial sandstone bodies and red silty clays up to 450 m thick. The Hortigüela Formation (300 m maximum thick) is composed of oncolitic limestones, marls, silty clays, and small lenses of sandstone with abundant faunas (ostracodes, and bone fragments) and floras (charophytes and blue-green algae). Both units yield charophytes of Late Hauterivian to Early Barremian age (Martín-Closas and Alonso Millán 1998). Depositional Sequence 6 (DS-6) consists of the Pantano de la Cuerda del Pozo Formation, which is Barremian in age. It contains lenticular bodies of sandstones, conglomerates, clays, and silts and thin limestones beds, deposited in a complex basin-axial fluviatile system with multistoried unconfined channels migrating in a wide alluvial plain (Clemente and Pérez-Arlucea 1993). Depositional Sequence 7 (DS-7) consists of the Abejar and Castrillo de la Reina formations, both of fluviatile origin and Late Barremian–Aptian in age. The first formation was deposited in a complex basin-transverse alluvial system, mainly braided rivers. The second unit represents more distal meandering rivers. This sequence appears basinwide, with greatest thickness in both western and eastern Cameros (close to 2000 m) and is the main infill of the largest depocenters of the basin.

From the analysis of 15 stratigraphic sections in the study area, two transects (N–S and NNE–SSW trending) of the above stratigraphic units were constructed (Figs. 3, 4). There is clearly a major increase in thickness of the main units to the north. This suggests that active local normal faults exerted major control on the configuration of secondary depocenters in this area of the basin, and influenced the architecture of stratigraphic units and depositional sequences (Mas et al. 1993; Guimerà et al. 1995). These normal faults are antithetic to the extensional ramp that was forming the Cameros Basin (Guimerà et al. 1995).

PROCEDURES

To characterize the detrital modes of the clastic intervals from the depositional sequences in the western Cameros Basin, a total of sixty-nine samples of medium-grained sandstone were collected along stratigraphic sections close to the localities of Hortezuelos (AHE), Peñacoba (PEÑ), Campolara (CML), Rupelo (RUP), Brezales (BRZ), La Gallega (GAS and GAN), Moncalvillo (MON), Castrovido (CTV), and Terrazas (TRZ and TRR) (see Figs. 1, 3, and 4 for locations). In addition, two sandstone samples were collected from the underlying marine formation (Talveila Formation) for comparison with the syn-rift units. Samples were impregnated with blue epoxy resin before thin-section grinding. Thin sections were etched and stained using HF and sodium cobaltinitrite for potassium feldspar, and alizarin-red and potassium ferrocyanide for carbonate identification (Chayes 1952, and Lindholm and Finkelman 1972, respectively). Quantitative petrographic analysis was performed by point counting thin

←

FIG. 3.—N–S trending stratigraphic transect A of uppermost Jurassic–Lower Cretaceous formations, depositional sequences, and their relations in the western Cameros Basin, with location of samples. Fa and Fb indicate location of deduced basement faults. HIN, Hinojosa section; AHE, Arroyo del Helechal section; PEÑ, Peñacoba section; CON, Contreras section; CML, Campolara section; CUB, Cubillejos section; RUP, Rupelo section. See Figure 1 for location of sections.

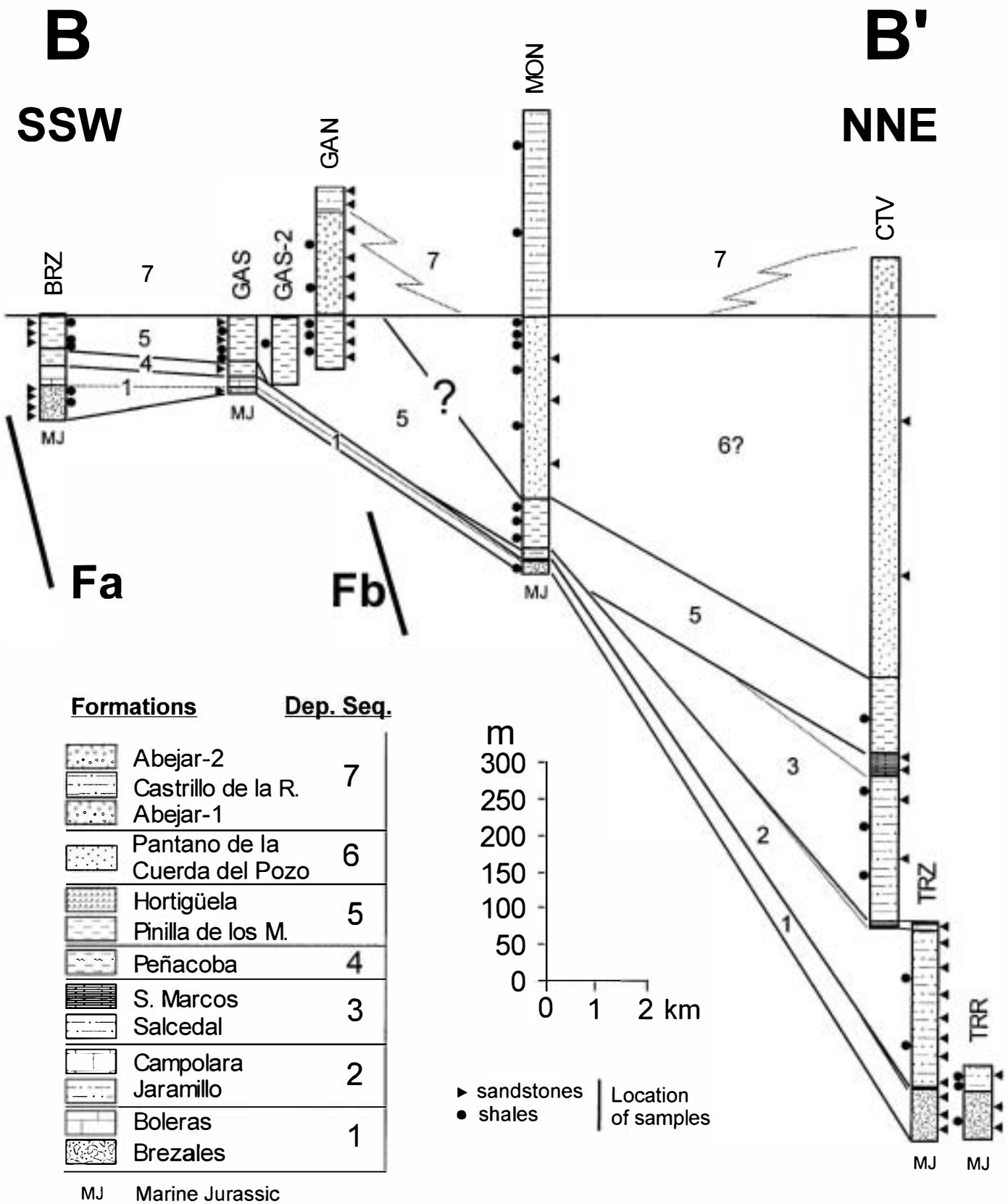

FIG. 4.—NNE–SSW trending stratigraphic transect B of uppermost Jurassic–Lower Cretaceous formations, depositional sequences, and their relations in the western Cameros Basin, with location of samples. Fa and Fb indicate location of deduced basement faults. BRZ, Brezales section; GAS, La Gallega southern section; GAN, La Gallega northern section; MON, Moncalvillo section; CTV, Castrovido section; TRZ and TRR, Terrazas section. See Figure 1 for location of sections.

TABLE 1.—*Key to counted petrographic classes and recalculated parameters.*

NCE (Non-Carbonate Extrabasinal)	Qt	Qmr	Monocrystalline quartz, undulosity < 5°	Recalculated parameters	
		Qmo	Monocrystalline quartz, undulosity > 5°		
		Qp2–3	Polycrystalline quartz with 2–3 subgrains	Q	Qmr + Qmo + Qp2–3 + Qp > 3c Qp > 3f + Cq + Ch
		Qp > 3c	Polycrystalline quartz with >3 subgrains (>0.062 mm)	F	Ks + Kfi + Ck + Ps + Pfi + Cp + Po3
		Qp > 3f	Polycrystalline quartz with >3 subgrains (0.062–0.030 mm)	R	Qfrm + Qfrg + Qfrs + Kfrg + Pfrg + Lm + Mfrm + CE
		Qfm	Quartz in low and medium metamorphic rock fragment		
		Qfrg	Quartz in plutonic/gneiss rock fragment	Qm	Qmr + Qmo + Qp2–3 + Qp > 3c + Qfrm + Qfrg + Qfrs + Cq
		Qfrs	Quartz in sandstone rock fragment	F	Ks + Kfrg + Kfi + Ck + Ps + Pfrg + Pfi + Cp + Po3
		Cq	Carbonate replacement on quartz	Lt	Qp > 3f + Ch + Lm + Ml + Sc + Md + Sd + Fo + Oss
	K	Ks	K-feldspar, single crystals	Qm	Qmr + Qmo + Qp2–3 + Qp > 3c + Qfrm + Qfrg + Qfrs + Cq
		Kfrg	K-feldspar in plutonic/gneiss rock fragment	K	Ks + Kfrg + Kfi + Ck
		Kfi	Clay minerals replacement on K-feldspar	P	Ps + Pfrg + Pfi + Cp
		Ck	Carbonate replacement on K-feldspar		
				Qmr	Qmr
	P	Ps	Plagioclase, single crystals	Qmo	Qmo
		Pfrg	Plagioclase in plutonic/gneiss rock fragment	Qp	Qp2–3 + Qp > 3c + Qp > 3f
		Pfi	Clay minerals replacement on plagioclase		
		Cp	Carbonate replacement on plagioclase	Lm	Lm
				Lsm	Ml + Md
L		Ch	Chert (>3 subgrains <0.030 mm)	Lse	Sc + Sd + Fo + Oss
		Lm	Schist-slate		
				Rg	Qfrg + Kfrg + Pfrg
	M	Ms	Muscovite	Rs	Qfrs + CE
		Bi	Biotite	Rm	Qfrm + Lm + Mfrm
		Mfrm	Mica in metamorphic rock fragments		
				P/F	(Ps + Pfrg + Pfi + Cp)/(Ks + Kfrg + Kfi + Ck + Ps + Pfrg + Pfi + Cp)
		Hm	Heavy minerals		
				I.V.	Intergranular volume: (Cm + Po) − Po3
CE (Carbonate Extrabasinal)	Ls	Ml	Micritic limestone		
		Sc	Sparry limestone		
		Md	Dolomicrite		
		Sd	Dolosparite		
		Fo	Fossils		
		Css	Carbonate cement in sandstone		
NCI (Non-Carbonate Intrabasinal)			Rip-up clasts		
CI (Carbonate Intrabasinal)		In	Micritic fragments		
		Bi	Bioclasts		
Cm (Cements)		Cm1	Carbonate cement		
		Cm2	Quartz plus K-feldspar cements		
		Cm3	Kaolinite plus illite cements		
		Cm4	Fe-oxide cement		
Po (Porosity)		Po1	Primary porosity		
		Po2	Secondary porosity after intergr cement		
		Po3	Secondary porosity after feldspar		

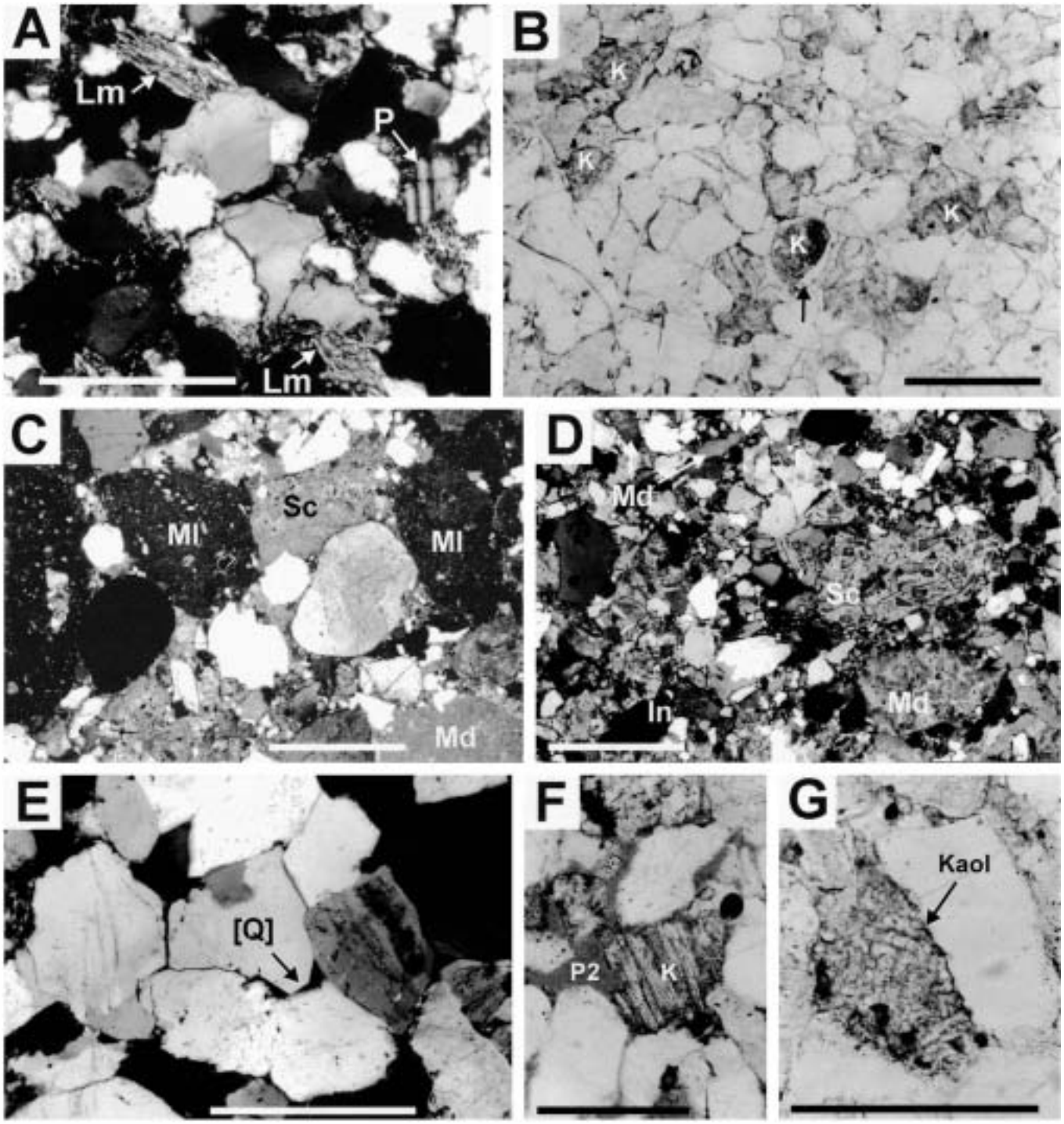

FIG. 5.—Thin-section photomicrographs of detrital components and diagenetic features in southern Cameros sandstones. Scale bar in all photographs is 0.3 mm. A) Medium-grained sandstone from Jaramillo Formation (sample TRZ-11, DS-2, petrofacies B) showing a quartzose framework with plagioclase grains (P) and metamorphic lithic fragments (Lm). The framework exhibits dense packing generated by compaction. This process also produces diagenetic matrix (pseudomatrix) by mechanical compaction of Lm grains (lower right). Cross-polarized light. B) Well-sorted medium-grained arkose from Castrillo de la Reina Formation (sample PEÑ-8, DS-7, petrofacies D). Conspicuous long and concave–convex grain-to-grain contacts suggest that chemical compaction occurred. K-feldspar (K) commonly appears with syntaxial overgrowths (arrow). Plane-polarized light. C) Litharenite from Brezales Formation (sample AHE-8, DS-1, petrofacies A), in which carbonate rock fragments are the main detrital components: micritic limestone (Ml), micritic dolostone (Md), and sparitic limestone. Poorly sorted framework shows a dense fabric due to compaction of carbonate sedimentary rocks. Note that roundness of quartz grains varies strongly, suggesting a recycled origin. Cross-polarized light. D) Litharenite from Brezales Formation (sample TRZ-3, DS-1, petrofacies A) exhibiting a poorly sorted framework and a great variety of carbonate grains. Coarse-grained limestone (Sc) shows a foraminifera grainstone microfacies of marine Jurassic provenance. Fine-grained dolostones (Md) also are present in variable grain size and with peloidal microfacies. Carbonate intrabasinal grains (In) also are exhibit intense compaction. Cross-polarized light. E) Quartz cement overgrowths ([Q]) in a subarkose from Abejar Formation (sample GAN-13, DS-7, petrofacies D). Note the abundance of monocrystalline quartz grains. Fitted fabric is due to quartz cement overgrowths that produce straight contacts between cement crystals. Also, primary porosity is preserved. Cross-polarized light. F) Partial dissolution of K-feldspar grain (honeycomb texture), causing secondary porosity (P2) in a

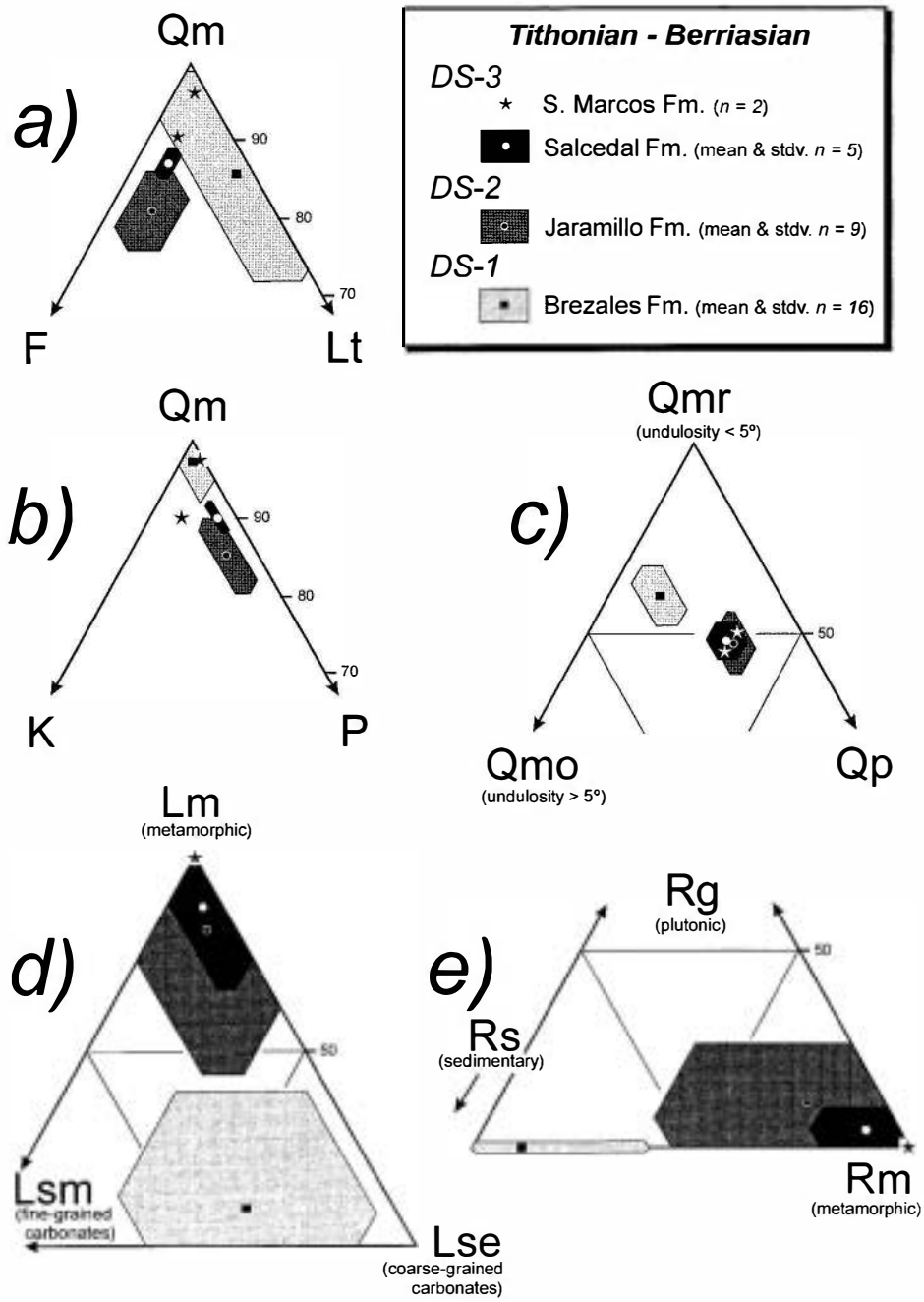

FIG. 6.—Ternary plots describing sandstone composition from the Brezales, Jaramillo, Salcedal, and San Marcos formations. Values of mean and standard deviation are represented by dots and polygons, respectively. See Table 1 for an explanation of petrographic parameters.

sections using the ''Gazzi–Dickinson method'' (Ingersoll et al. 1984), and according to the petrographic groups defined by Zuffa (1980) (Table 1). In this way, it also is possible to treat the framework data according to the ''traditional'' method (Pettijohn 1957) or the ''Indiana School'' (Ingersoll et al. 1984). These methods differ in the concept of the unit to be counted. In the ''Gazzi–Dickinson'' methodology, monominerals are sand-size grains (0.062–2 mm) including those constituents of large polycrystalline sand-size grains. In addition, lithic fragments consist of sand-size grains constituted by crystals < 0.062 mm in size. However, the ''traditional'' methodology considers the entire sand-size detrital units, irrespectively of the size of their mineral constituents, emphasizing the textural and compositional information of the detrital population.

A total of 400 to 500 points were counted per slide, including framework and intergranular space components. Postdepositional modifications of the original framework (i.e., feldspar dissolution or feldspar replacement) were considered and evaluated. Because the main object of this paper was to

←

subarkose from Abejar Formation (sample PEÑ-2, DS-7, petrofacies D). Plane-polarized light. G) Face-to-face kaolinite (kaol) replacement after a K-feldspar grain (epimatrix). Dark areas are stained K-feldspar remains. Note that this kaolinite corresponds to the Kfi petrographic class in Table 1. Pantano de la Cuerda del Pozo Formation (sample CTV-26, DS-6, petrofacies D). Plane-polarized light.

infer provenance, an attempt was made to restore the original framework composition, with a view to achieving correct interpretations based on that restored composition (McBride 1985).

The mineralogical study of the clayey and marly samples was carried out by means of X-ray diffraction (XRD) analysis. The bulk composition was determined using the powder diffraction method, after grinding and homogenizing the samples to < 53 μm. For the study of the phyllosilicates, the < 20 μm fraction was chosen instead of the clay fraction (< 2 μm) in order to gain information on the detrital components. Samples containing carbonates were treated with 5% acetic acid and washed with deionized water. After separation of the < 20 μm fraction using differential tubes, oriented aggregates were prepared by sedimentation onto glass slides and were subjected to thermal treatment at 550°C for 2 hours and to solvation with ethylene glycol. Non-oriented powders and phyllosilicate aggregates of each sample were examined in a Siemens D500 diffractometer equipped with a graphite monochromator using the Siemens SOCABIM Diffract AT3.3 software.

GRAIN TYPES, INTERGRANULAR COMPONENTS, AND POROSITY

Thirty-nine petrographic classes were recognized in the point counting, referring to detrital grains (32), intergranular components (4), and porosity (3) (Table 1). Following criteria of Zuffa (1980), detrital classes can be grouped into four categories: noncarbonate extrabasinal (NCE), carbonate extrabasinal (CE), noncarbonate intrabasinal (NCI), and carbonate intrabasinal (CI). Detrital grains in sandstones are mainly of extrabasinal origin, providing detailed information of their source rocks.

Noncarbonate Extrabasinal Grains (NCE).—This group includes a wide variety of quartz, K-feldspar, plagioclase, fine-grained lithic fragments, mica, and dense minerals (Qt, K, P, L, M, and HM, respectively, in Table 1). Quartz is the dominant component (more than 70%) and is present as monomineralic grains or as quartz constituents of coarse polymineralic grains. Monomineralic quartz grains are monocrystalline nonundulose (Qmr), monocrystalline undulose (Qmo), and the polycrystalline varieties Qp2–3 and Qp > 3, following the criteria of Basu et al. (1975). Qmr is the more abundant quartz type, commonly constituting 50% of total quartz grains. In addition, we have split the Qp > 3 class into two different classes: Qp > 3c and Qp > 3f, as a function of subgrain size. Thus, Qp > 3c represents polycrystalline grains with more than three subgrains greater than 0.062 mm in size. The size of subgrains in the Qp > 3f class is between 0.062 mm and 0.030 mm. Notice that Qp2–3 and Qp > 3c varieties are included in the Qm category, following Dickinson (1985, p. 335). However, the Qp > 3f class must be included into the Lt category because their subgrains do not exceed 0.062 mm in size (Zuffa 1980; Dickinson 1985). K-feldspar and plagioclase are subordinate and generally do not exceed 25% of total detrital components (Fig. 5A, B). Both minerals also are present in coarse-grained rock fragments. Clay minerals and carbonate replacements on feldspar (Fig. 5G) also are included in these groups (Kfi, Pfi, Ck, and Cp in Table 1). Noncarbonate lithic fragments (L) are fine-grained (< 0.062 mm) metamorphic fragments that include slate and fine-grained schists (Lm) (Fig. 5A), and chert grains (Ch). Chert grains (subgrains < 0.030 mm in size) appear without any clear texture (e.g., organic ghosts) to ascribe this class to a sedimentary origin. Noncarbonate lithic fragments always are present but in scarce percentages (less than 5% of total grains). We distinguish between "lithic" (L grains) and "rock" fragment (R grains); these terms refer to fine-grained ("lithic") or coarse-grained plus fine-grained polymineralic ("rock" fragment) fragments, respectively. The former are the lithic grains defined by the Gazzi–Dickinson method (L), and the latter refer to the traditional sense of rock fragment (R) (Suttner et al. 1981; Ingersoll et al. 1984).

Carbonate Extrabasinal Grains (CE).—This group includes a great variety of sedimentary carbonate grains from Triassic and Jurassic marine formations. They are fine grained limestones (Ml) and dolostones (Md) (Fig. 5C) and coarse-grained limestones (Sc) and dolostones (Sd) (Fig. 5D). In addition, fossils (Fo) and carbonate cement in sandstone grains (Css) were included in this group. The latter class is an "R" grain (coarse-grained sedimentary grain) following the traditional methodology but a "CE" grain using the Gazzi–Dickinson methodology. Cavazza et al. (1993) showed the relevance of this petrographic class when sandstones break up into individual grains to produce recycled detrital components and monocrystalline calcite grains. Carbonate extrabasinal grains are abundant in some samples, constituting up to 30% of total grains, but are absent in other samples. This group of components is considered to be sedimentary lithic fragments (Ls) and combines with noncarbonate lithic fragments (L) and Qp > 3f to make up the total lithic population (Lt).

Noncarbonate Intrabasinal and Carbonate Intrabasinal Grains (NCI and CI).—These groups of clasts are not very abundant (mean of 3%) and consist of inorganic grains of carbonate and noncarbonate nature and bioclasts (mainly characea, ostracodes, and gastropods). They are recognizable following the criteria of Zuffa (1985). These grains have not been considered in any recalculated parameter (Table 1) because their origin is not related to any source rock but to the basin deposits themselves. Noncarbonate intrabasinal grains (NCI, rip-up clasts) commonly are associated with quartzofeldspathic deposits, whereas carbonate intrabasinal, both bioclasts (Bi) and micritic fragments (In) (Fig. 5D), generally are present in sedimentolithic sandstones.

Intergranular Components and Porosity.—In addition to the grain petrographic classes, some categories have been used to evaluate cements (carbonate, quartz, K-feldspar, clay minerals, and Fe oxide) and porosity (primary, secondary after cements, and secondary after feldspar grains). Cements are well represented in Cameros sandstones, ranging from 5% to 33% of total rock volume. Carbonate cement is widely present, but mainly in sedimentolithic sandstones. Quartz and K-feldspar overgrowths and clay-mineral pore fillings are commonly present in quartzofeldspathic sandstones (Fig. 5B, E). In order to identify primary and secondary porosity we used the criteria of Schmidt and McDonald (1979a, 1979b). Secondary porosity (Fig. 5F) is very important in quartzofeldspathic sandstones, with the dissolution of K-feldspar being the principal variety (maximum, 7%). Primary porosity always is present but in low percentages (mean, 3%). Intergranular volume in the sandstones (cements plus primary porosity) provides information about compaction. Intergranular volume ranges from 12% to 32%. The variation is due mainly to the interplay of two processes: (1) the action of mechanical and chemical compaction, which reduces intergranular volume, and (2) early cementation by carbonate, which inhibits compaction.

Recalculated Parameters.—These parameters refer to detrital point-count data and are shown in Table 1. They are obtained following the criteria of Pettijohn et al. (1972) (QFR), Dickinson (1985) (QmFLt; QmKP), Dickinson (1970) (P/F), Basu et al. (1975) (Qmr/Qmo/Qp), Arribas et al. (1990), and Critelli and Le Pera (1994) (RgRsRm). In addition, we used the LmLsmLse ternary diagram to contrast the content of metamorphic lithic fragments (Lm) with respect to the content of fine-grained carbonate lithic fragments (Lsm) and coarse-grained carbonate lithic fragments (Lse). All of these recalculated parameters were used to plot recalculated modes in the ternary diagrams presented in Figures 6, 7, and 8. Notice that values in the QFR diagram (Pettijohn et al. 1972) are not expressed graphically but are used in the text to describe sandstone composition with a nomenclature of regular usage (e.g., arkose, litharenite, quartz arenite).

SANDSTONE COMPOSITION

Depositional Sequences 1, 2, and 3

The sandstone framework composition of the detrital units (Brezales, Jaramillo, and Salcedal formations) of these depositional sequences is very quartzose (> 75% quartz grains) with variable amounts of feldspar and rock fragments (Fig. 6). Minor variations in sandstone composition between

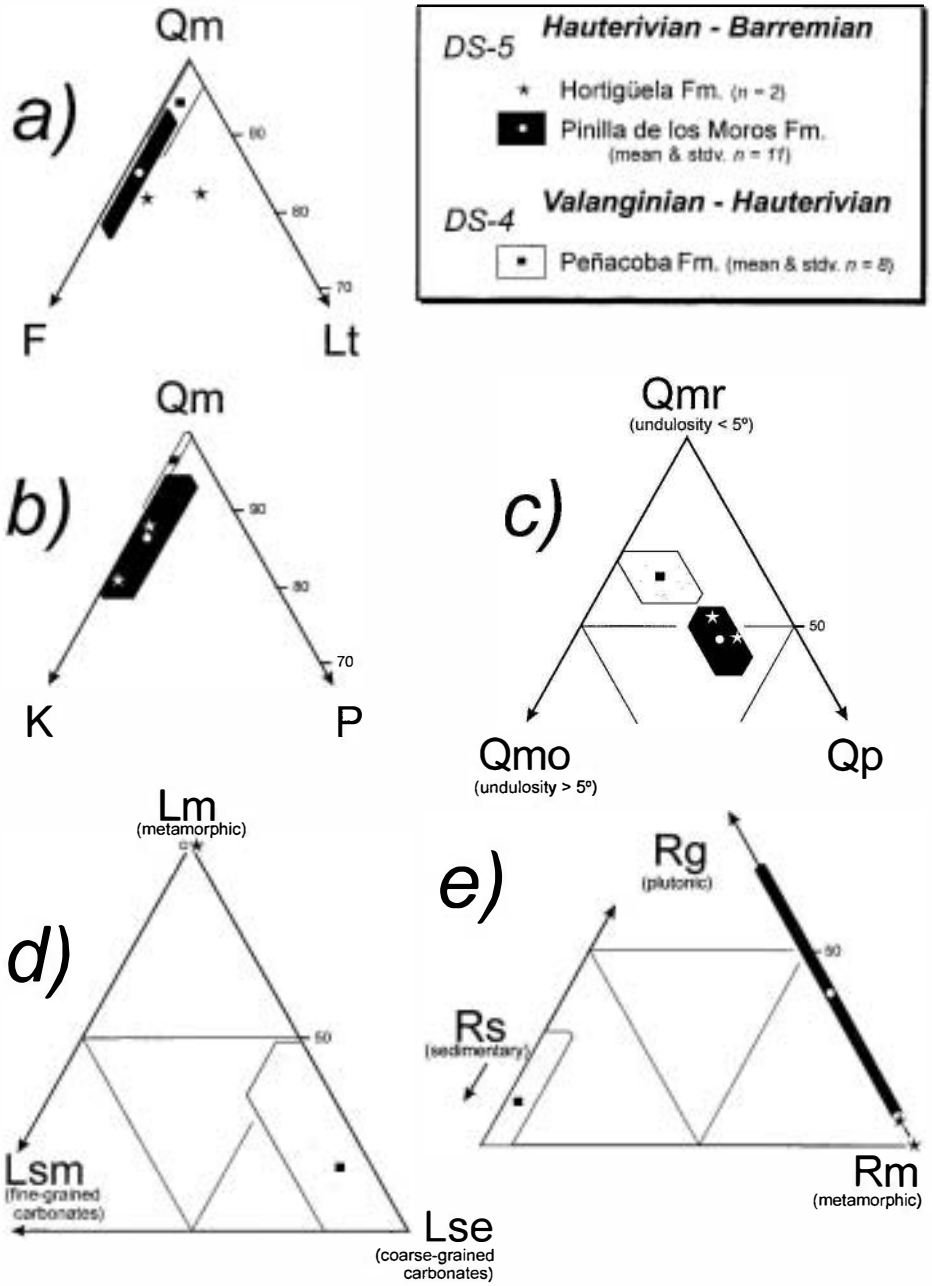

FIG. 7.—Ternary plots describing sandstone composition from the Hortigüela, Pinilla de los Moros and Peñacoba formations. Values of mean and standard deviation are represented by dots and polygons, respectively. See Table 1 for an explanation of petrographic parameters.

units reflect changes in the nature of detritus during sedimentation. Types of postdepositional modification during burial include variable compaction (mean intergranular volumes of 24%, 21%, and 23% in the Brezales, Jaramillo, and Salcedal formations, respectively) manifested by mechanical deformation of ductile grains (intrabasinal carbonate clasts and mica) and by pressure-solution features between carbonate and quartz grains and minor quartz-to-quartz contacts. Calcite and dolomite cements are the most common diagenetic phases. Kaolinite pore filling and replacements (epimatrix after feldspar) and quartz overgrowths also are developed at the top of the Brezales Formation and in the Jaramillo and Salcedal formations.

Brezales Formation.—Clast-supported conglomerates with carbonate pebbles are the main lithofacies of this unit, which has infiltrated sandy matrix whose grains have the same compositions as interbedded sandstones. The latter are sedimentary litharenites (sedarenites) and quartz arenites with variable amounts of sedimentary carbonate grains (CE). The siliciclastic population is made up mainly of well rounded monocrystalline quartz grains. These grains commonly exhibit embayments probably related to leaching episodes in a soil environment (Johnsson 1990). In the northern sector (RUP and TRZ sections), at the top of this unit, mica (muscovite and biotite), K-feldspar, plagioclase, and metamorphic lithic fragments appear in low proportions. Intrabasinal carbonate clasts (CI) with charophytes are locally very abundant and appear to be affected by ductile deformation. Sedimentary lithic fragments (fine-grained and coarse-grained carbonates, Lsm and Lse, respectively) dominate the lithic population, indicating a sedimenticlastic origin of this unit (mean value of $Lm_{10}Lsm_{34}Lse_{56}$, Fig. 6). In addition, coarse-grained sandstone fragments are common (mean of 8%). The shaly and marly layers are predominantly composed of calcite, quartz, and occasionally minor amounts of plagioclase and hematite. The clay-mineral assemblage includes illite, kaolinite, and randomly interlayered illite–smectite mixed-layer clays (Table 2).

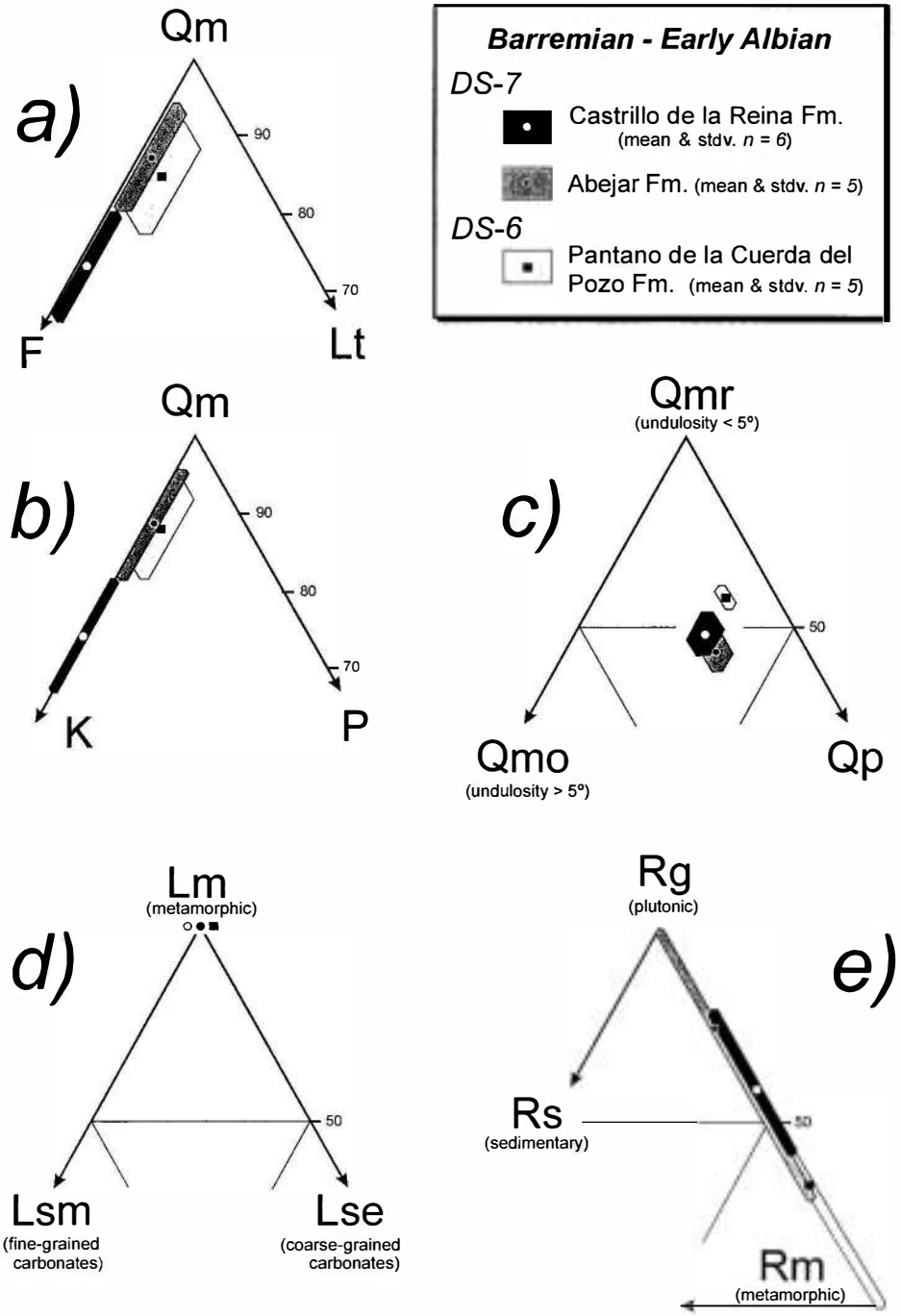

FIG. 8.—Ternary plots describing sandstone composition from the Pantano de la Cuerda del Pozo, Abejar, and Castrillo de la Reina formations. Values of mean and standard deviation are represented by dots and polygons, respectively. See Table 1 for an explanation of petrographic parameters.

Interpretation.—The underlying marine Jurassic deposits are the main source of Brezales Formation. The proportions of quartz in the sandstones of Brezales Formation are very similar to those of older Jurassic formations (Talveila Formation, in Table 3) and are characterized by a predominance of the more stable monocrystalline grain type ($Qmr_{60}Qmo_{28}Qp_{12}$, Fig. 6C). Q/L ratios in sandstones vary spatially and are interpreted as local variations in composition of the bedrock. Thus, siliciclastic rocks appear to be the dominant sources in the southern area (AHE and BRZ sections), whereas carbonate rocks are a more important source of sediments in the northern area (RUP and TRZ sections). In the more deeply subsiding trench (northern part of the basin) and at the top of the unit, there is an important change of provenance with the introduction of feldspatholithic sediments from low-grade metamorphic terranes.

Jaramillo Formation.—Sandstones in this unit are subarkoses ($Q_{81}F_{13}R_6$) with dominantly metamorphic and rare sedimentary lithic fragments (mean value of lithics, $Lm_{81}Lsm_7Lse_{12}$; Fig. 6D). Plagioclase is the dominant feldspar ($Qm_{86}K_3P_{11}$; Fig. 6B), appearing as twinned and untwinned grains of albite. Low-grade to medium-grade metamorphic lithic grains (Lm) mainly include slates and micaschists. Sedimentary lithic fragments consist of fine-grained and coarse-grained dolostones and sparitic limestones and can be locally important (as much as 9% of bulk framework), especially in the lower part of this unit and along the northern trench

TABLE 2.—*Variation in the mineral composition of the lutitic and marly samples.*

Depositional Sequence	Formation	Sample	Quartz	Calcite	Dol	Plag	Feld	Hem	Illite	Chlor.	I/S	Kaol
DS-7	Castrillo de la Reina	PEÑ-9	****				*	*	***			*
		PEÑ-7	****				*	*	***			*
		PEÑ-4	****				*	*	***			*
		MON-33	****	*				*	***		*	**
		MON-32	****				*	*	***			*
		GAN-25	****				*	*	***			**
		GAN-22	****				*	*	***			**
	Abejar	GAN-15	****				*		****			***
		GAN-10	****				*		**			****
DS-6	Pantano de la Cuerda del Pozo	MON-26	****	*				*	***		**	*
		MON-22	****	***					***		*	**
		MON-21	****					*	**		**	**
		MON-19	****						***			**
		MON-17	****	***				*	**		*	**
DS-5	Pinilla de los Moros	MON-13	****	*	**		*	*	***	**	**	
		MON-9	****	**	*		*	*	***	**		
		MON-7	****	**	*		*	*	***	**	**	
		RUP-42	****	**		*		*	***			
		CTV-16	****						***			**
		BRZ-30	****			*			***			**
		BRZ-20	****	*	*	*			***			*
		BRZ-17	****						***			*
		GAS-15	****				*		***			**
		GAS-11	****				*		***	**		**
		GAS-9	**	****	**				***	**		
		GAS-101	****		*		*	*	***			**
		GAN-8	****	*			*		***		*	****
		GAN-6	****	*			*	*	**			***
		GAN-2	****						***			**
DS-4	Peñacoba	AHE-26	****	***			*	*			*	***
		AHE-16	*	****			*		*		*	**
		AHE-14		****					*		*	**
DS-3	Salcedal	RUP-21	****	*			*	*	***	**		
		RUP-19	****	*		*			***	****		
		CML-9	***	****					***		*	
		CTV-10	****	*		**		*	***		*	**
		CTV-7	****			**			***			
		CTV-3	****	**		*		*	***	**		
DS-2	Jaramillo	TRR-11	****	**		*		*	**	*		
		TRR-9	****	*	**	*			***	**		
		TRZ-21	****	*		*		*	**	**		
		TRZ-12	****	**		*		*				
DS-1	Brezales	BRZ-12	*	****							**	*
		BRZ-4	****	**							**	*
		TRR-4	****	***		*		*	**		***	***
		RUP-12	***	****		*		*	***			**
		RUP-7	****	**		*			***	**		
		MON-1	***	****				*	***		**	***
		CML-4	**	****							**	**

Quartz, calcite, dolomite (Dol.), plagioclase (Plag.), feldspar (Feld.), and hematite (Hem.) contents were estimated from X-ray diffraction traces of unoriented mineral-aggregate samples, whereas the phyllosilicate contents were calculated from oriented aggregates of the <2μm fraction. Chlor. = chlorite; I/S = irregular illite-smectite mixed-layers; Kaol. = kaolinite. Major phase (****), frequent phase (***), minor phase (**), accessory phase (*)

(RUP and TRZ sections). Other detrital constituents are micas (muscovite and biotite), dense minerals (zircon, tourmaline, anatase, and opaques), argillaceous to silty rip-up clasts, and micritic carbonate intraclasts. The shaly and marly samples contain quartz, calcite, plagioclase, and minor amounts of hematite and dolomite. Illite and chlorite are the only phyllosilicates present in these samples (Table 2).

Interpretation.—The petrographic characteristics of the sandstone framework, together with the clay-mineral assemblage of the shales, suggest that the Jaramillo Formation was derived mainly from low-grade to medium-grade metamorphic and minor sedimentary rocks. The large polycrystalline quartz population ($Qmr_{48}Qmo_{17}Qp_{35}$, Fig. 6C), the presence of micas, and the high P/F values (mean of 0.75) all confirm the predominance of metamorphic sources for this unit.

Salcedal Formation.—These sandstones are subarkoses with a greater quartz population than the underlying Jaramillo Formation sandstones ($Q_{87}F_9R_4$). Twinned and untwinned albite grains predominate over K-feldspar grains ($P_{99}K_2P_8$; Fig. 6B). Metamorphic lithic fragments (slates and mica schists) dominate the lithic population ($Lm_{87}Lsm_5Lse_8$; Fig. 6D). Extrabasinal and intrabasinal carbonates (CE and CI, respectively) are very scarce, appearing at the base of the unit and decreasing to near zero towards the top. Other framework grains are micas (muscovite and biotite) and dense minerals (rutile, tourmaline, and opaque minerals) in very minor proportions. The shales contain quartz, calcite, plagioclase, and scarce hematite, with illite as the main clay mineral. Chlorite is present in three samples, with kaolinite and randomly interlayered illite–smectite mixed-layer clays as minor constituents (Table 2).

Interpretation.—Quartzofeldspathic petrofacies of sandstone from this unit suggest a provenance mainly from low-grade to medium-grade metamorphic sources. The scant input from sedimentary rocks is present only at the base of the unit. The similarity of the P/F value (mean, 0.79) and the proportions of quartz types ($Qmr_{49}Qmo_{18}Qp_{33}$; Fig. 6C) confirm that the source areas are equivalent to those of Jaramillo Formation. However, Salcedal Formation sandstones exhibit a more compositionally mature framework than Jaramillo Formation sandstones, manifested by a high proportion of Qm (Fig. 6A, B) and the loss of unstable sedimentary lithic fragments (Fig. 6D).

San Marcos Formation.—This unit constitutes the upper part of DS-3 and consists mainly of lacustrine carbonate deposits. However, in the CRV section, fluviodeltaic sandstone bodies appear interbedded with lacustrine carbonates. These sandstones have a siliciclastic framework composition

with a quartz arenite composition ($Q_{91}F_4R_5$). P/F values (mean, 0.58) indicate a slight predominance of plagioclase over K-feldspar, but given the scant presence of these minerals in the framework, this conclusion may not be statistically significant. Lithic fragments are predominantly slates, schists, and minor amounts of metamorphic chert, frequently associated with abundant mica grains. Proportions of quartz grain types are equivalent to those of sandstones from the underlying Jaramillo and Salcedal formations (Fig. 6C).

Interpretation.—The petrographic characteristics of the sandstones suggest that the sources of San Marcos Formation were low-grade to medium-grade metamorphic rocks. A high proportion of quartz grains lacking signs of having been recycled from older sedimentary sources indicates considerable maturation of these deposits during transport.

Depositional Sequence 4

Peñacoba Formation.—Sandstones in this unit consist of quartz arenites and minor subarkoses (mean of $Q_{95}F_3R_2$), commonly cemented by siderite and dolomite containing pseudomorphs of kaolinite. Authigenic K-feldspar and quartz overgrowths have been observed at the top of the unit. These early diagenetic phases retard the effects of compaction on the framework, and deformation features are less common in these sandstones than in underlying units. The quartz population is characterized by rounded grains with a predominance of monocrystalline types ($Qmr_{63}Qmo_{25}Qp_{12}$; Fig. 7C). These grains commonly exhibit abraded overgrowths, indicating a recycled origin. The minor feldspar population consists solely of K-feldspar grains ($Qm_{97}K_3P_0$; Fig. 7B). The concentration of this component is highest at the top of the sequence. Lithic grains are very scarce, consisting mainly of coarse-grained carbonate rock fragments (Lse; Fig. 7D). Metamorphic lithic fragments (Lm) and fine-grained carbonate rock fragments (Lsm) are present in trace amounts. Carbonate intrabasinal grains (CI) are common (mean, 4.5% from total grains) and consist mainly of bioclasts (characeas, ostracodes), oncoids, and soft micritic grains. Only three shaly samples were analysed from this formation, and they are composed of calcite, quartz, scarce feldspar, and hematite. The clay-mineral assemblage consists mainly of kaolinite with minor proportions of illite and randomly interstratified mixed-layer illite–smectite (Table 2).

Interpretation.—This unit falls into the ''stable craton'' provenance type following Dickinson et al. (1983) (Fig. 7A). The presence of abundant features of recycling processes (i.e., rounded monocrystalline quartz grains, inherited quartz cements, presence of carbonate rock fragments) strongly suggests that the origin of this sequence may be related to erosion of older Jurassic, and probably Triassic, siliciclastic (arkosic) and carbonate formations.

Depositional Sequence 5

Pinilla de los Moros Formation.—Sandstones are quartz arenites and subarkoses (mean of $Q_{86}F_{13}R_1$) with very minor concentrations of rock fragments. The intergranular volume is occupied by kaolinite, quartz, and carbonate (ferroan dolomite) cements. Other diagenetic features include replacement of feldspars by carbonates and clay minerals, especially kaolinite (epimatrix), and dissolution of the former. Chemical compaction (pressure-solution processes) is manifested by well developed long, concave-convex contacts between quartz grains. The framework composition is quartzofeldspathic (mean, $Qm_{85}F_{13}Lt_2$; Fig. 7A) with abundant polycrystalline quartz (Fig. 7C). Qm dominates over feldspar ($Qm_{87}K_{11}P_2$, Fig. 7B), with a dominance of K-feldspar over plagioclase (mean P/F of 0.24). At the top of the unit (RUP section) there is a considerable decrease in feldspar. The lithic content is represented exclusively by fine-grained slate schists and chert grains (Fig. 7A, D). Phaneritic rock fragments (Rg—coarse-crystalline quartz-feldspar grains) also are present and may exceed the proportions of the aphanitic metamorphic population (Fig. 7E). Muscovite also is present in trace amounts. Intrabasinal grains include fine-grained carbonates, bioclasts (characeas), and kaolinite rip-up clasts. Shales and marls analyzed contain predominantly quartz, with minor proportions of calcite, K-feldspar (or plagioclase), and less commonly, hematite and dolomite. The clay-mineral assemblage is dominated by illite and kaolinite, although samples from the MON section contain significant amounts of chlorite and randomly interstratified mixed-layer illite–smectite instead of kaolinite (Table 2).

Interpretation.—The quartzofeldspathic character of the sandstones suggests a dominant first-order supply from granite-gneiss source rocks (i.e., ''craton interior'' provenance type of Dickinson et al. 1983). The presence of minor metamorphic lithic fragments in the framework indicates additional input from low-grade metamorphic sources. The absence of recycling features in quartz grains (e.g., inherited quartz cements) or of any carbonate rock fragment suggests that sedimentary terrains were not an important source of sediments during deposition of this unit. The evolution of sandstone composition towards more mature deposits at the top of the unit (decrease in feldspar content in RUP section) may be related to sediment maturation during transport when tectonic activity slowed down.

Hortigüela Formation.–Detrital beds are scarce in this unit, and thus only two samples from CML section were analyzed. They come from two thin, fine-grained sandstone intervals interbedded with oncoid limestones and marls. The framework is quartzofeldspathic with a substantial concentration of lithic fragments and micas (mean, $Qm_{81}F_{11}Lt_8$; Fig. 7A). In addition, there are important similarities with the underlying Pinilla de los Moros Formation sandstones, such as the P/F ratio (mean, 0.10; Fig. 7B), the proportions of quartz types (Fig. 7C), and the absence of sedimentary lithics (Fig. 7D).

Interpretation.—We can assume that the sandstone petrofacies from this unit are similar to those from the previous formation. The differences are (1) a greater proportion of metamorphic lithic fragments and (2) the virtual absence of coarse-grained rock fragments in sandstones from the Hortigüela Formation (Fig. 7A, E). Inferences similar to those deduced to Pinilla de los Moros Formation can be drawn for this unit. The greater content of metamorphic lithic fragments may be related to reactivation of the feeder system providing metamorphic supplies. However, these compositional differences between units could also be produced by the effects of finer grain sizes on the framework composition of the Hortigüela Formation sandstones.

Depositional Sequence 6

Pantano de la Cuerda del Pozo Formation.—Sandstones in this unit are subarkoses with small amounts of rock fragments ($Q_{84}F_{11}R_5$). Compaction is the main diagenetic process affecting framework grains, and is manifested by grain-fracture and pressure-solution processes. Thus, the intergranular volume is low (mean, 16.5%), and contains quartz and minor carbonate cements, and low porosity. The rock-fragment population consists of fine-grained metamorphic rock fragments (slates and minor schists: Lm) and phaneritic granite-gneiss fragments (Rg in Fig. 8E). No fine-grained or coarse-grained sedimentary rock fragments are present. Feldspar commonly is replaced by kaolinite or partially dissolved, and consists mainly of K-feldspar (mean P/F value 0.19; Fig. 8B). The quartz population exhibits proportions of quartz types similar to those in DS-2, DS-3, and DS-5. The XRD analysis of shales reveals the presence of quartz, associated with calcite and hematite in some samples. The clay-mineral assemblage includes illite, kaolinite, and randomly interstratified mixed-layer illite–smectite (Table 2).

Interpretation.—Petrographic features of sandstones and the clay-mineral association from the Pantano Formation resemble those from DS-5 (Pinilla de los Moros and Hortigüela formations). Thus, DS-5 and DS-6 belong to the same petrofacies, and hence provenance of this unit, like

those of DS-5, is from erosion of equivalent crystalline bedrocks with minor low-grade metamorphic supplies.

Depositional Sequence 7

Abejar Formation.—Sandstones are medium-grained to coarse-grained subarkoses (mean, $Q_{88}F_{11}R_1$) with considerable reduction of intergranular volume (mean, 14%) by compaction. Breakage of grains and pressure-solution between quartz grains are very common. Feldspar commonly is replaced by kaolinite and then as deformed epimatrix. In addition, there is widespread occurrence of partial and total intrastratal dissolution of feldspar. Framework collapse features are very common. Cements are scarce, and there is only minor quartz overgrowth and kaolinite pore-filling cement. There is considerable primary porosity, partially increased and oversized by feldspar dissolution.

Sandstones are quartzofeldspathic (mean, $Qm_{88}F_{11}Lt_1$). Total lithic fragments (Lt) are mainly chert grains. The feldspar population is dominated by K-feldspar (mean P/F, 0.03; Fig. 8B). Coarse crystalline quartz-feldspar grains (Rg) are common, appearing in greater abundance than total metamorphic rock fragments (Rm—fine-grained plus coarse-grained fragments) (Fig. 8E). The proportions of quartz types (mean, $Qmr_{43}Qmo_{22}Qp_{35}$; Fig. 8C) do not differ substantially from the quartz populations from DS-2, DS-3, DS-5, and DS-6. Two shaly samples were analyzed within this unit, and both contain quartz and feldspar, together with illite and kaolinite.

Interpretation.—The provenance of the Abejar Formation represents sources from crystalline rocks, and differs from older petrofacies in that it is almost purely quartzofeldspathic, falling very close to the QmF edge on the QmFLt ternary diagram, and coarse crystalline rock fragments predominate over metamorphic. Thus, crystalline bedrock (granite-gneiss) was likely as the main source for this unit. Low-grade metamorphic supplies appear highly diluted by the quartzofeldspathic detritus.

Castrillo de la Reina Formation.—This unit is made up of red arkosic and subarkosic (mean, $Q_{72}F_{25}R_3$) sandstones interbedded with shales. The framework components are mainly medium-grained, and are moderately compacted (mean intergranular volume, 20.5%). Mica and rip-up clasts have undergone ductile deformation and pressure solution between adjacent quartz grains, manifested by elongate and embayed contacts. However, no extensive grain-fracture or collapse-framework features were observed. Common cement phases are quartz and K-feldspar as grain overgrowths, and minor kaolinite pore filling. The quartzofeldspathic framework composition is characterized by having the greatest proportion of feldspar of all the analyzed units (mean, $Qm_{73}F_{26}Lt_1$; Fig. 8A), and by the predominance of K-feldspar over plagioclase ($Qm_{74}K_{26}P_0$). The lithic population is composed mainly of accessory low-grade metamorphic (slate) grains. Nonfoliated and foliated coarse crystalline rock fragments (granite-gneiss and schists) also are present in minor amounts (Fig. 8E). The quartz population is composed predominantly of monocrystalline types, which very often exhibit subrounded-subangular sections with embayments filled by clayey material probably acquired in a soil environment prior to ultimate deposition (Johnsson 1990). The shaly samples consist of quartz, feldspar, and minor amounts of hematite, together with illite and kaolinite.

Interpretation.—Both the sandstone petrofacies and the clay-mineral assemblages of this unit can be interpreted as similar to those from Abejar Formation but with a greater feldspar content in framework sandstone. A basement uplifted provenance type can be deduced from the plot of sandstone composition in a QmFLt diagram (Dickinson et al. 1983). This unit was interpreted as the distal facies of the Abejar Formation (Mas et al. 1993). Compositional differences between the units can be explained as a product of diagenesis. Early diagenetic water, enriched in dissolved ions from K-feldspar leaching originated in the permeable Abejar Formation, could not produce extensive intrastratal dissolution of feldspars in Castrillo Formation distal deposits (Stanley and Benson 1979; Almon and Davies 1979). Moreover, early diagenetic water may have produced extensive K-feldspar overgrowths in Castrillo Formation sandstones.

DISCUSSION

Source Rocks and Tectonics

Sedimentary, low-grade to medium-grade metamorphic, and crystalline plutonic rocks are deduced to have been source rocks for the sequence examined, on the basis of the framework composition of sandstones and the clay-mineral assemblages of shales and marls in the western Cameros Basin.

The underlying marine Jurassic deposits are posited as the main sources during the first stage of sedimentation (Brezales Formation), producing quartzosedimentolithic petrofacies and clay-mineral assemblages dominated by randomly interstratified mixed-layer illite–smectite, illite, and kaolinite. This conclusion is supported by the similarities to the pre-rift Talveila unit in terms of quartz population and the presence of abundant carbonate rock fragments ascribed to marine carbonate facies. The local nature of the source is manifested by local variations in Q/L composition in sandstones. These sources were still active during the sedimentation of sequences DS-2, DS-3, and probably DS-4, but their debris appear progressively diluted by other sources of a metamorphic nature. Erosion of the Triassic red-bed succession could have provided the detritus during deposition of the Peñacoba Formation (DS-4). This unit is recycled, as evidenced by the analysis of quartz types and their heritage patterns (e.g., abraded overgrowths), the presence of carbonate rock fragments, and the low content of feldspar, indicating that the sources are from the base of the Mesozoic pile of sediments. There is no evidence of erosion of sedimentary bedrock during generation of DS-5, DS-6 and DS-7, so sedimentary sources can be considered to have been stripped away by that time.

Low-grade to medium-grade metamorphic sources are recognized in the sandstone framework from the top of DS-1 (Brezales Formation) to DS-7, manifested by the presence of metamorphic lithic fragments (Lm), plagioclase, micas, and coarse-grained rock fragments in minor amounts. The metamorphic character of the source for the DS-2 (Jaramillo Formation), DS-3 (Salcedal Formation), and part of DS-5 (Pinilla de los Moros Formation) also is evidenced by the presence of detrital illite and chlorite in the clay-mineral assemblage of the shales. Metamorphic source terranes may have been in the Hercynian Iberian Massif. The Paleozoic basement of the Cameros Basin corresponds to the West Asturian–Leonese Zone (Julivert et al. 1972) of the Iberian Massif (Fig. 9). This zone consists mainly of a thick lower Paleozoic sequence of slates and quartzites of greenschist metamorphic facies and minor amphibolite facies (Julivert 1983). Outcrops are located in the NW of the Iberian Peninsula and in the inner part of the Cameros Basin (Fig. 9). This structural zone represents the principal low-grade to medium-grade metamorphic source that fed the basin during deposition of DS-2 and DS-3.

Crystalline plutonic rocks are well represented in the Central Iberian Zone of the Hesperian Massif (Julivert et al. 1972). This zone is located to the SW of the West Asturian–Leonese Zone, and the limit between the two zones is located in the SW of the Cameros Basin (Fig. 9). Hercynian granites, granodiorites, and gneisses are the main bedrock lithologies in the Central Iberian Zone, with minor exposures of low-grade metamorphic rocks (Villaseca et al. 1993). This zone is the likely main source area for detrital sediments from DS-5, DS-6, and DS-7, whose compositions are characteristically quartzofeldspathic for the sandstones, and by the presence of kaolinite and illite in the shales, which in addition contain almost no calcite.

The location of the inferred sources and their activity during the infill of the basin imply that metamorphic detritus from the West Asturian–Leonese Zone came from the NW as axial transport along the main subsiding troughs during final deposition of DS-1 and throughout sedimentation of DS-2 and DS-3. Plutonic crystalline sources in the Central Iberian Zone

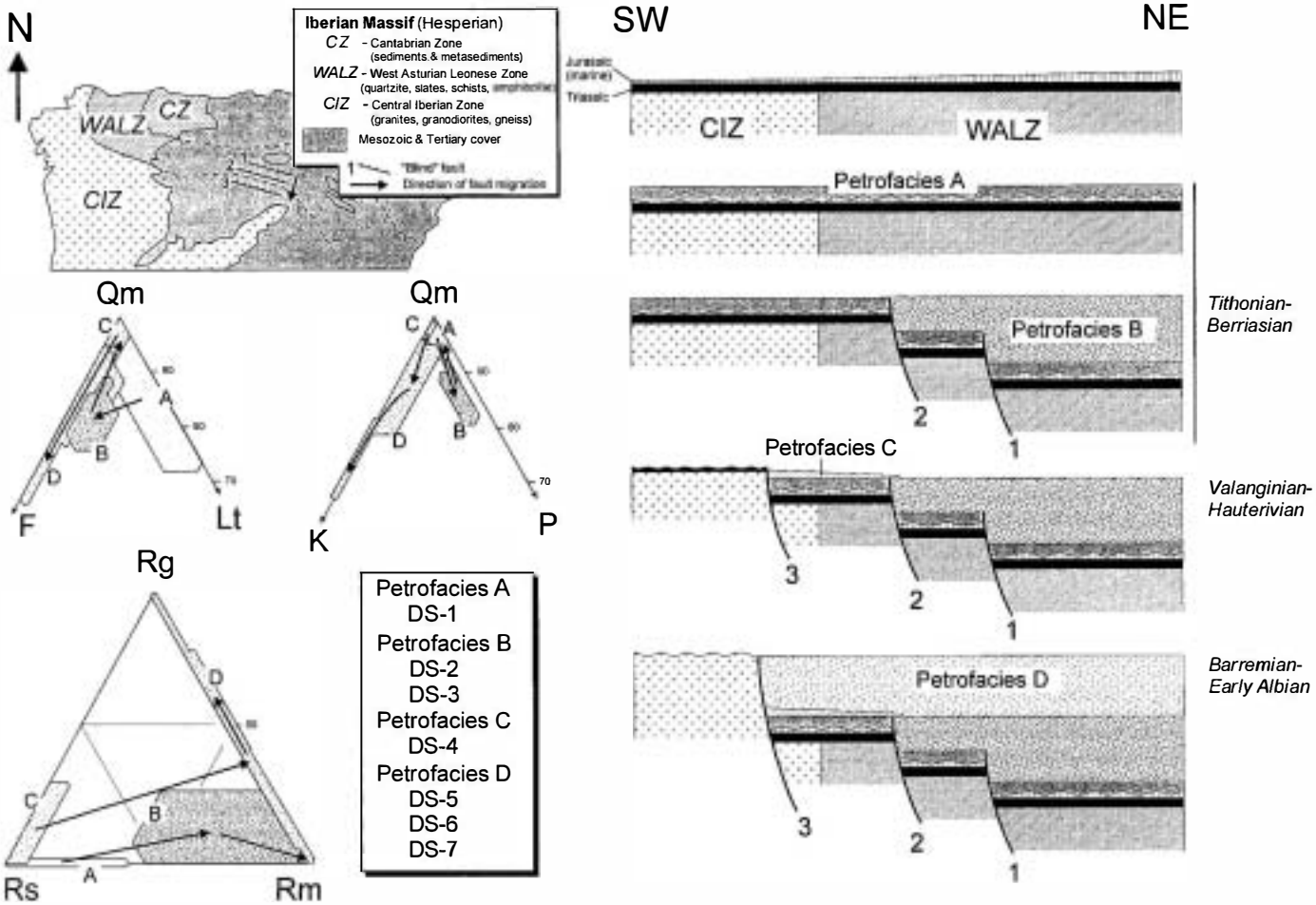

FIG. 9.—Evolution of petrofacies during Late Jurassic–Middle Albian clastic deposition in the western Cameros Basin and their genetic and tectonic relationships with the Iberian Massif zones. Arrows in ternary diagrams show the evolution of petrofacies through time. See Table 1 for an explanation of petrographic parameters. Note that marine Jurassic deposits are poorly represented in the Central Iberian Zone.

supplied quartzofeldspathic detritus during the last episode of rifting, probably owing to the propagation of normal faults to the SW (Mas et al. 1993), generating troughs that affected the Central Iberian Zone.

Activity of the feeder systems from a given source rock does not imply the elimination of the previously active source, but rather the dilution of a former source by input of new detrital material. Thus, the important role of plutonic sources during DS-5, DS-6, and DS-7 does not require the extinction of low-grade and medium-grade metamorphic basement as a source area, which was active during DS-2 and DS-3 time. Granite-gneiss bedrock can produce much more sand-size detritus than slate–schist (Palomares and Arribas 1993), and thus, the mixing of products from equivalent plutonic and slate–schist outcrop areas produces considerable dilution of low-grade and medium-grade metamorphic supplies by the voluminous quartzofeldspathic sediments furnished by plutonic rock types.

Petrofacies and Depositional Sequences

On the basis of compositional framework similarities, sandstones can be classified into four main petrofacies.

Petrofacies A.—This petrofacies consists of quartzosedimentolithic sandstones. They are sedarenites and quartz arenites that record erosion of siliciclastic and carbonate marine Jurassic pre-rift cover rocks. This petrofacies was developed during deposition of the Brezales Formation and coincides very closely with sequence DS-1.

Petrofacies B.—Sandstones of petrofacies B are quatzofeldspathic, with plagioclase as the main feldspar, micas, and metamorphic lithic fragments. They may also contain sedimentary rock fragments. The inferred sources are low-grade to medium-grade metamorphic terranes of the West Asturian–Leonese Zone in the Hesperian Massif. This petrofacies is characteristic of the detrital units in sequences DS-2 and DS-3 (Jaramillo, Salcedal, and San Marcos formations).

Petrofacies C.—These sandstones are slightly feldspathic quartz arenites. Their chief petrographic characteristics are the presence of sedimentary carbonate fragments, the absence of plagioclase, and abundant features of recycling manifested on quartz grains. The origin of this petrofacies is related to recycling from sedimentary sources (mainly Triassic arkoses), and it formed during deposition of the Peñacoba Formation (DS-4).

Petrofacies D.—These sandstones are quartzofeldspathic with very minor amounts of metamorphic lithic fragments, and low P/F values. The deduced parent rocks are mainly coarse crystalline plutonic rocks located in the Central Iberian Zone at the SW of the basin. Petrofacies D accumulated during deposition of DS-5, DS-6, and DS-7.

The preceding analysis shows that the petrofacies coincide with depositional sequences and their hierarchy. These petrofacies are not biased by grain-size effects, because only medium grained sandstones were examined, in order to avoid the grain-size influence on composition (Zuffa 1985). Petrofacies A (DS-1) accumulated during initial rift deposition, and was derived from local sources in the underlying sedimentary substrate. Petrofacies B records new input of metamorphic detritus from the West Astu-

TABLE 3.—*Values of mean and standard deviation for recalculated parameters for sandstones from the various detrital formations.*

	Talveila		Brezales		Jaramillo		Salcedal		E. Marcos		Peñacoba	
	X	d1	X	d1	X	d1	X	d1	X	d1	X	d1
Q	100.0	0.0	85.0	14.2	80.9	5.1	87.4	2.0	91.7	5.8	95.3	6.9
F	0.0	0.0	2.0	5.1	13.4	4.2	9.0	1.7	3.9	3.4	3.1	5.9
R	0.0	0.0	13.0	14.3	5.7	2.7	3.6	0.7	4.4	3.4	1.6	1.5
NCE	100.0	0.0	82.8	19.7	96.5	8.1	99.5	1.0	100.0	0.0	94.2	12.2
CE	0.0	0.0	10.5	12.4	1.3	3.0	0.3	0.6	0.0	0.0	1.2	1.1
CI	0.0	0.0	5.7	11.8	2.2	5.1	0.2	0.5	0.0	0.0	4.5	12.1
Qm	100.0	0.0	85.2	13.6	80.8	5.1	87.2	2.0	91.9	3.4	94.7	7.6
F	0.0	0.0	2.0	5.2	13.8	4.7	9.1	1.8	4.0	3.5	3.3	6.2
Lt	0.0	0.0	12.8	13.6	5.4	3.4	3.7	0.9	4.2	0.1	2.0	1.7
Qm	100.0	0.0	97.9	5.5	85.4	4.9	90.5	1.9	95.9	3.6	96.6	6.5
K	0.0	0.0	0.8	1.9	3.3	1.6	1.9	0.5	2.3	2.8	3.4	6.4
P	0.0	0.0	1.3	3.6	11.3	5.1	7.6	2.2	1.8	0.8	0.0	0.1
Qmr	59.6	3.8	68.4	7.8	48.0	8.2	49.9	4.7	48.8	3.9	63.3	7.2
Qmo	33.4	3.2	28.2	4.4	17.1	4.2	18.5	4.7	17.1	3.4	25.1	7.7
Qp	6.9	0.7	11.4	8.2	34.9	8.8	32.7	4.7	34.1	0.5	11.6	12.3
Lm	—	—	10.6	28.8	81.1	37.8	86.7	21.7	100.0	0.0	16.7	21.9
Lvm	—	—	33.6	28.0	6.7	30.0	5.3	7.7	0.0	0.0	7.1	12.2
Lse	—	—	55.8	30.3	12.2	26.2	8.0	17.9	0.0	0.0	76.2	21.3
Rg	—	—	0.0	0.0	10.5	14.4	3.9	5.9	0.0	0.0	11.2	20.1
Rs	—	—	88.9	29.4	18.2	37.0	7.9	13.5	0.0	0.0	86.7	22.7
Rm	—	—	11.1	29.4	71.2	33.8	88.2	11.9	100.0	0.0	2.0	5.4
P/F	—	—	0.18	0.31	0.75	0.12	0.79	0.08	0.58	0.31	0.00	0.01

	Pinilla de los Moros		Hortigüela		Pantano		Abejar		Castrillo de la Reina	
	X	d1	X	d1	X	d1	X	d1	X	d1
Q	85.6	8.3	78.0	8.5	84.3	9.4	87.7	7.9	72.0	7.5
F	12.9	7.8	10.4	4.3	11.0	6.1	11.1	7.8	24.7	6.9
R	1.5	1.0	11.6	4.8	4.7	4.2	1.2	1.8	3.3	0.9
NCE	97.3	8.7	100.0	0.0	100.0	0.0	100.0	0.0	100.0	0.0
CE	0.0	0.0	0.0	0.0	0.0	0.0	0.0	0.0	0.0	0.0
CI	2.7	8.7	0.0	0.0	0.0	0.0	0.0	0.0	0.0	0.0
Qm	85.2	8.6	81.5	0.0	84.9	7.3	87.5	6.8	73.4	7.5
F	13.1	7.9	10.6	4.6	11.3	6.2	11.2	7.8	25.6	7.1
Lt	1.7	0.9	7.9	4.5	3.8	2.5	1.3	1.0	1.0	0.8
Qm	86.8	8.1	88.6	4.4	88.2	6.7	88.7	7.1	74.1	7.3
K	11.5	9.0	10.4	4.2	10.0	5.6	11.0	6.8	25.8	7.2
P	1.8	2.8	1.1	0.1	1.8	1.9	0.3	0.9	0.1	0.1
Qmr	45.9	8.9	49.2	3.0	57.5	3.2	43.1	6.4	53.5	5.1
Qmo	19.7	5.1	16.3	2.4	12.9	1.3	22.0	3.6	19.3	4.5
Qp	34.3	9.8	34.4	5.4	29.6	3.4	34.9	4.9	27.2	3.3
Lm	100.0	0.0	100.0	0.0	100.0	0.0	100.0	0.0	100.0	0.0
Lvm	0.0	0.0	0.0	0.0	0.0	0.0	0.0	0.0	0.0	0.0
Lse	0.0	0.0	0.0	0.0	0.0	0.0	0.0	0.0	0.0	0.0
Rg	39.4	32.7	3.3	4.7	32.4	34.2	68.1	38.6	61.2	19.1
Rs	0.0	0.0	0.0	0.0	0.0	0.0	0.0	0.0	0.0	0.0
Rm	60.6	32.7	96.7	4.7	67.6	34.2	31.9	38.6	38.8	19.1
P/F	0.24	0.35	0.10	0.03	0.19	0.19	0.03	0.06	0.08	0.08

rian–Leonese Zone into the most deeply subsiding troughs at the north end of the study area, which produced a thick section during sequences DS-2 and DS-3 (Fig. 4). This axial supply of metamorphic detritus is in addition to local supply of sedimentary detritus. Although DS-2 and DS-3 correspond to petrofacies B, minor compositional variations are apparent in Fig. 6. These variations in composition do not represent significant changes in source, but a more mature stage for DS-3 sandstones. This may be a product of diminishing relief and an increasing duration of sediment weathering during pedogenesis, transport, and deposition (Mack 1978; Johnsson et al. 1991). Consequently, DS-1, DS-2, and DS-3 effectively represent a megacycle generated during the first stage of northern subsiding troughs (Mas et al. 1993), and is characterized by the presence of petrofacies A at the base and petrofacies B at the top.

Petrofacies C, developed in the Peñacoba Formation (DS-4), also represents recycled deposits from the lower Mesozoic sedimentary cover (Triassic) in the SW part of the study area, indicating propagation of NW–SE-trending normal faults that bounded the newly generated troughs. Arkosic petrofacies D (DS-5, DS-6, and DS-7) corresponds to new input of granitic detritus from the Central Iberian Zone. Thus, a second megacycle can be defined which consists of DS-4 to DS-7 and is recorded in the succession from petrofacies C at the base to petrofacies D at the top. In addition, minor variations in sandstone composition are observed in the detrital units of petrofacies D (Figs. 7, 8), consisting of a progressive increase in the concentration of K-feldspar and phaneritic coarse crystalline rock fragments. These upward variations to less mature deposits might be related to such factors as the increase of source area relief (Stallard 1985; Retallack 1990) during the deposition of successive sequences, representing increased tectonic activity in the source regions, favoring conditions of weathering-limited erosion.

Analysis of petrofacies in intraplate rift basins and their relation to depositional sequences demonstrates that the source-rock signal is dominant in controlling sandstone composition, and thus, a good correlation between petrofacies and depositional sequence boundaries exists. Tectonism is the main factor that controls the architecture (Prosser 1993) and composition of the basin fill. The evolution of intraplate rift basins is related to the propagation of trough-bounding normal faults. Thus, the nature of erosional sources of sediments (flank uplifts) may change with time as a function of the position of faults and distribution of rock types in the source area. In the Cameros Basin, the structure and composition of the basement (Hesperian Massif) played a decisive role in the distribution of petrofacies through time. Environmental modification of sandstone composition also is inferred, but as a secondary influence. Maturation of sandstone deposits at the top of some depositional sequences (e.g., DS-3) may correspond to transport processes and sediment reworking during tectonically quiet intervals. Intervals with strong tectonic activity also are recorded at the tops of some depositional sequences (e.g., DS-7) and are manifested as immature sandstone deposits. This close relationship between petrofacies and tectonics may contribute to a better understanding of the tectonic evolution of rift basins.

In addition, clay minerals from the interbedded shales maintain the source signal related to the corresponding petrofacies. Thus, petrofacies related to recycling sediments (petrofacies A and C) are characterized by interbedded shales with a wide variety of clay minerals (illite, kaolinite, and randomly interlayered illite–smectite mixed-layer clays). Petrofacies B is characterized by the presence of chlorite in interbedded shales provided by the metamorphic sources from the Western Asturian–Leonese Zone. Illite and kaolinite are the dominant clay minerals in shales associated with petrofacies D, as feldspar weathering products of crystalline sources from the Central Iberian Zone.

Finally, general models of the provenance of sand and sandstone based on framework composition suggest that quartzofeldspathic sandstone is typical in "basement uplifted" tectonic settings (Dickinson and Suczek 1979; Dickinson et al. 1983). However, in the Cameros Basin recycled petrofacies

(quartzosedimentolithic or quartzarenithic) from the previous sedimentary cover are developed at the base of each megacycle (petrofacies A and C, respectively) and precede the main quartzofeldspathic infill. The presence of these recycled deposits has been observed by other authors in equivalent tectonic settings (i.e., Zuffa et al. 1980).

CONCLUSIONS

The composition of sandstone from the western Cameros Basin (Upper Jurassic to Middle Albian) permits the characterization of depositional sequences in terms of source lithology, paleogeography, and paleotectonic evolution of the basin.

Two major megacycles can be established: (1) Tithonian to Berriasian, comprising depositional sequences 1, 2, and 3; and (2) Valanginian to Middle Albian, comprising depositional sequences 4, 5, 6, and 7. Both megacycles start with a quartzolithic petrofacies generated by erosion of Mesozoic pre-rift sedimentary cover and evolve to quartzofeldspathic petrofacies produced by erosion of the Hercynian basement (Hesperian Massif).

The first megacycle records the initial stage of rifting with the presence of basal quartzosedimentolithic ($Qm_{85}F_2Lt_{13}$) sandstones derived from the erosion of marine Jurassic pre-rift deposits (DS-1; Brezales Formation; petrofacies A). The overlying depositional sequences (DS-2 and DS-3) are characterized by quartzofeldspathic petrofacies ($Qm_{81}F_{14}Lt_5$ and $Qm_{87}F_9Lt_4$, respectively; petrofacies B) with predominance of plagioclase over K-feldspar (P/F = 0.75–0.79). This last petrofacies is related to the erosion of low-grade to medium-grade metamorphic terranes from the West Asturian–Leonese Zone of the Hesperian Massif. Input from this source produced progressive dilution of detritus from the sedimentary cover. Evolution of sandstone composition from DS-1 to DS-3 reflects a slowing of tectonic activity, as indicated by the increased compositional maturity of sediments toward the top of the megacycle.

The second megacycle starts with a quartzarenite ($Qm_{95}F_3Lt_2$) petrofacies (DS-4; Peñacoba Formation; petrofacies C), which records erosion of Triassic arkoses and associated carbonates from the SW of the basin. The rest of depositional sequences (DS-5, DS-6, and DS-7: Pinilla de los Moros–Hortigüela, Pantano, and Abejar–Castrillo de la Reina formations) correspond to quartzofeldspathic petrofacies (petrofacies D) with predominance of K-feldspar over plagioclase ($Qm_{88-73}F_{11-26}Lt_{1-8}$; P/F = 0.0–0.24). These deposits record the erosion of plutonic rocks from the Central Iberian Zone in the Hesperian Massif. The evolution of sandstone composition in this megacycle indicates a progressive increase in tectonic activity with time, with the presence of less mature (more feldspathic) deposits towards the top of the megacycle (DS-7; Table 3, Fig. 9).

The petrographic characteristics of the megacycles are related to the paleogeographic configuration and evolution of the Cameros Basin. The first megacycle (Tithonian–Berriasian) developed in NW–SE-trending troughs generated in the West Asturian–Leonese Zone. Migration and stepping of normal faults to the SW created similarly trending troughs, developed on crystalline basement of the Central Iberian Zone (Fig. 9).

Finally, we stress the importance of information that can be obtained from sandstone petrofacies in this kind of basin, where tectonism governs the creation of depositional sequences. The close correlation between petrofacies and depositional sequences promotes sandstone composition as a powerful tool for interpretation of depositional sequences. Petrofacies analysis also can contribute to paleogeographic and paleotectonic reconstructions. Traditional petrographic criteria, which consist largely of considering fine-grained and phaneritic rock fragments, have proved very useful. The RmRsRg ternary diagram in particular offers useful discriminating power in analysis of the evolution of sandstone modes in rifted basins. In addition, the information provided by clay-mineral analysis of the shales and marls associated with the sandstones has proven to be an important tool supporting the interpretations derived from sandstone petrography.

ACKNOWLEDGMENTS

This work was funded by the Spanish Dirección General de Investigación Científica y Técnica (Projects PB97-0298 and BTE2001-0026). We are grateful to Associate Editor M. Johnsson and referees R. Dorsey, E.F. McBride, and G.G. Zuffa for reviews and helpful comments and suggestions.

The data of point counting have been achieved, and are available in digital form, at the World Data Center-A for Marine Geology and Geophysics, NOAA/NGDC, 325 Broadway, Boulder, CO 80303; (phone: 303-497-6339; fax: 303-497-6513; E-mail: wdcamgg@ngdc.noaa.gov; URL: http://www.ngdc.noaa.gov/mgg/sepm/jsr/).

REFERENCES

Almon, W.R., and Davies, D.K., 1979, Regional diagenetic trends in the Lower Cretaceous muddy sandstones, Powder River Basin, *in* Scholle, P.A., and Schluger, P.R., eds., Aspects of Diagenesis: SEPM, Special Publication 26, p. 379–400.

Alonso-Azcárate, J., Arche, A., Barrenechea, J.F., López-Gómez, J., Luque, F.J., and Rodas, M., 1997, Paleogeographical significance of the clay minerals in the Permian and Triassic sediments of the SE Iberian Ranges, Eastern Spain: Palaeogeography, Palaeoclimatology, Palaeoecology, v. 136, p. 309–330.

Arribas, J., Gómez-Gras, D., Rosell, J., and Tortosa, A., 1990, Estudio comparativo entre las areniscas Paleozoicas y Triásicas de la Isla de Menorca: Evidencias de procesos de reciclado: Revista de la Sociedad Geológica de España, v. 3, p. 105–116.

Basu, A., Young, S.W., Suttner, L.J., James, C.W., and Mack, G.H., 1975, Re-evaluation of the use of undulatory extinction and polycrystallinity in detrital quartz provenance interpretation: Journal of Sedimentary Petrology, v. 45, p. 873–882.

Blatt, H., 1967, Provenance determination and the recycling of sediments: Journal of Sedimentary Petrology, v. 37, p. 1031–1044.

Cavazza, W., Zuffa, G.G., Camporesi, C., and Ferretti, C., 1993, Sedimentary recycling in a temperate climate drainage basin (Senio River, north-central Italy): Composition of source rock, soil profiles, and fluvial deposits, *in* Johnsson, M.J., and Basu, A., eds., Processes Controlling the Composition of Clastic Sediments: Geological Society of America, Special Paper 284, p. 247–261.

Chayes, F., 1952, Notes on the staining of potash feldspar with sodium cobaltonitrite in thin section: American Mineralogist, v. 37, p. 337–340.

Clemente, P., and Perez-Arlucea, M., 1993, Depositional architecture of the Cuerda del Pozo Formation, Lower Cretaceous of the extensional Cameros Basin, North-Central Spain: Journal of Sedimentary Petrology, v. 63, p. 437–452.

Critelli, S., 1999, The interplay of lithospheric flexure and thrust accommodation in forming stratigraphic sequences in the southern Apennines foreland basin system, Italy: Lincei Scienze Fisiche e Naturali, Rendiconti, serie IX, v. 10, p. 257–326.

Critelli, S., and Le Pera, E., 1994, Detrital modes and provenance of Miocene sandstones and modern sands of the Southern Apennines thrust-top basins (Italy): Journal of Sedimentary Research, v. A64, p. 824–835.

DeCelles, P.G., and Hertel, F., 1989, Petrology of fluvial sands from the Amazonian foreland basin, Peru and Bolivia: Geological Society of America, Bulletin, v. 101, p. 1552–1562.

Dickinson, W.R., 1970, Interpreting detrital modes of graywacke and arkose: Journal of Sedimentary Petrology, v. 40, p. 695–707.

Dickinson, W.R., 1985, Interpreting provenance relations from detrital modes of sandstones, *in* Zuffa, G.G., ed., Provenance of Arenites: Dordrecht, The Netherlands, D. Reidel, p. 333–361.

Dickinson, W.R., and Suczek, C.A., 1979, Plate tectonics and sandstone compositions: American Association of Petroleum Geologists, Bulletin, v. 63, p. 2164–2182.

Dickinson, W.R., Beard, L.S., Brakenridge, G.R., Erjavec, J.L., Ferguson, R.C., Inman, K.F., Knepp, R.A., Lindberg, F.A., and Ryberg, R.T., 1983, Provenance of North American Phanerozoic sandstones in relation to tectonic setting: Geological Society of America, Bulletin, v. 94, p. 222–235.

Fontana, D., Zuffa, G.G., and Garzanti, E., 1989, The interaction of eustacy and tectonism from provenance studies of the Hecho Group Turbidite Complex (South-Central Pyrenees, Spain): Basin Research, v. 2, p. 223–237.

Gazzi, P., 1966, Le arenarie del flysch sopracretaceo dell'Appennino modenese; correlazioni con il Flysch di Monghidoro: Mineralogica et Petrographica Acta, v. 12, p. 69–97.

Guimerà, J., Alonso, A., and Mas, R., 1995, Inversion of an extensional-ramp basin by a newly formed thrust: The Cameros basin (N Spain), *in* Buchanan, J.G., and Buchanan, P.G., eds., Basin Inversion: Geological Society of London, Special Publication 88, p. 433–453.

Hiscott, R.N., Wilson, R.C.L., Gradstein, F.M., Pujalte, V., García-Mondejar, J., Boudreau, R.R., and Wishart, H.A., 1990, Comparative stratigraphy and subsidence history of Mesozoic rift basins of North Atlantic: American Association of Petroleum Geologists, Bulletin, v. 74, p. 60–76.

Ingersoll, R.V., 1978, Petrofacies and petrologic evolution of the Late Cretaceous fore-arc basin, northern and central California: Journal of Geology, v. 86, p. 335–352.

Ingersoll, R.V., Bullard, T.F., Ford, R.L., Grimm, J.P., Pickle, J.D., and Sares, S.W., 1984, The effect of grain size on detrital modes: a test of the Gazzi–Dickinson point-counting method: Journal of Sedimentary Petrology, v. 54, p. 103–116.

Johnsson, M.J., 1990, Overlooked sedimentary particles from tropical weathering environments: Geology, v. 18, p. 107–110.

Johnsson, M.J., 1993, The system controlling the composition of clastic sediments, *in* Johnsson, M.J., and Basu, A., eds., Processes Controlling the Composition of Clastic Sediments: Geological Society of America, Special Paper 284, p. 1–19.

Johnsson, M.J., Stallard, R.F., and Lundberg, N., 1991, Controls on the composition of fluvial

sands from a tropical weathering environment: Sands of the Orinoco River drainage basin, Venezuela and Colombia: Journal of Geology, v. 96, p. 263–277.

JULIVERT, M., 1983, La estructura de la Zona Asturoccidental-Leonesa, *in* Geología de España. Libro Jubilar J.M. Ríos: Iustituto Geológico y Minero de España, T1, p. 381–407.

JULIVERT, M., FONTBOTÉ, J.M., RIBEIRO, A., AND NABAIS CONDE, L.E., 1972, Mapa tectónico de la Península Ibérica y Baleares, E. 1:1.000.000: Iustituto Geológico y Minero de España, Madrid.

LEEDER, M.R., 1995, Continental rifts and proto-oceanic rift troughhs, *in* Busby, C.J., and Iugersoll, R.V., eds., Tectonics of Sedimentary Basins: Oxford, U.K., Blackwell Science, p. 119–148.

LINDHOLM, R.C., AND FINKELMAN, R.B., 1972, Calcite staining: semiquantitative determination of ferrous iron: Journal of Sedimentary Petrology, v. 42, p. 239–245.

MACK, G.H., 1978, The survivability of labile light mineral grains in fluvial, eolian and littoral marine environments: The Permian Cutler and Cedar Mesa Formation, Moab, Utah: Sedimentology, v. 25, p. 587–606.

MARTÍN-CLOSAS, M., AND ALONSO MILLÁN, A., 1998, Estratigrafía y Bioestratigrafía (Charophyta) del Cretácico inferior en el sector occidental de la Cuenca de Cameros (Cordillera Ibérica): Revista de la Sociedad Geológica de España, v. 11, p. 253–269.

MAS, R., ALONSO, A., AND GUIMERÁ, J., 1993, Evolución tectonosedimentaria de una cuenca extensional intraplaca: La cuenca finijurásica–eocretácica de Los Cameros (La Rioja–Soria): Revista de la Sociedad Geológica de España, v. 6 p. 129–144.

MCBRIDE, E.F., 1985, Diagenetic proces ses that affect provenance determinations in sandstone, *in* Zuffa, G.G., ed., Provenance of Arenites: The Netherlands, Dordrecht, Reidel, p. 95–114.

PALOMARES, M., AND ARRIBAS, J., 1993, Modern stream sands from compound crystalline sources: Composition and sand generation index, *in* Johnsson, M.J., and Basu, A., eds., Processes Controlling the Composition of Clastic Sediments: Geological Society of America, Special Paper 284, p. 313–322.

PETTIJOHN, F.J., 1957, Sedimentary Rocks, 2nd Edition: New York, Harper, 718 p.

PETTIJOHN, F.J., POTTER, P.E., AND SIEVER, R., 1972, Sand and Sandstone: Berlin, Springer-Verlag, 618 p.

PROSSER, S., 1993, Rift-related linked depositional system and their seismic expression, *in* Williams, G.D., and Dobb, A., eds., Tectonics and Seismic Sequence Stratigraphy: Geological Society of London, Special Publication 71, p. 35–66.

RETALLACK, G.J., 1990, Soils of the Past; An Iutroduction to Paleopedology: Boston, Unwin Hyman, 520 p.

SALAS, R., GUIMERÁ, J., MAS, R., MARTÍN-CLOSAS, C., MELÉNDEZ, A., AND ALONSO, A., 2001, Evolution of the Mesozoic Central Iberian Rift System and its Cenozoic inversion (Iberian Chain), *in* Ziegler, P.A., Cavazza, W., Robertson, A.H.F., and Crasquin-Soleau, S., eds., Peri-Ihethyan Rift/Wrench Basins and Passive Margins: Musénm National D'Histoire Naturelle, Mémoires, t. 186, Peri-Tethys Memoir 6, p. 145–186.

SCHWAB, F., 1986, Sedimentary "signatures" of foreland basin assemblages: real or counterfeit?, *in* Allen, P.A., and Homewood, P., eds., Foreland Basins: Iuternational Association of Sedimentologists, Special Publication 8, p. 395–410.

SCHMIDT, V., AND MCDONALD, D.A., 1979a, The role of secondary porosity in the course of sandstone Diagenesis, *in* Scholle, P.A., and Schluger, P.R., eds., Aspects of diagenesis: SEPM, Special Publication 26, p. 175–207.

SCHMIDT, V., AND MCDONALD, D.A., 1979b, Texture and recognition of secondary porosity in sandstones, *in* Scholle, P.A., and Schluger, P.R., eds., Aspects of diagenesis: SEPM, Special Publication 26, p. 209–225.

STALLARD, R.F., 1985, River chemistry, geology, geomorphology, and soils in the Amazon and Orinoco basins, *in* Drever, J.I., ed., The Chemistry of Weathering: The Netherlands, Dordrecht, Reidel, p. 293–316.

STANLEY, K.O., AND BENSON, L.V., 1979, Early diagenesis of high plains tertiary vitric and arkosic sandstone, Wyoming and Nebraska, *in* Scholle, P.A., and Schluger, P.R., eds., Aspects of diagenesis: SEPM, Special Publication 26, p. 401–424.

SUTTNER, L.J., BASU, A., AND MACK, G.H., 1981, Climate and the origin of quartz arenites: Journal of Sedimentary Petrology, v. 51, p. 21–29.

VALLONI, R., 1985, Reading provenance from modern marine sands, *in* Zuffa, G.G., ed., Provenance of Arenites: The Netherlands, Dordrecht, Reidel, p. 309–332.

VILLASECA, C., BARBERO, L., HUERTAS, M.J., ANDONAEGUI, P., AND BELLIDO, F., 1993, A cross-section through Hercynian granites of the Central Iberian Zone: Excursion guide, Servicio de Publicaciones, Consejo Superior de Iuvestigaciones Científicas, Madrid, 122 p.

WILSON, R.C.L., WHITMARSH, R.B., TAYLOR, B., AND FROITZHEIM, N., EDS., 2001, Non-volcanic Rifting of Continental Margins; A Comparison of Evidence from Land and Sea: Geological Society of London, Special Publication 187, 585 p.

ZIEGLER, P.A., CAVAZZA, W., ROBERTSON, A.H.F., AND CRASQUIN-SOLEAU, S., EDS., 2001, Peri-Ihethyan Rift/Wrench Basins and Passive Margins: Muséum National D'Histoire Naturelle, Mémoires, t. 186, Peri-Tethys Memoir 6, 763 p.

ZUFFA, G.G., 1980, Hybrid arenites: their composition and classification: Journal of Sedimentary Petrology, v. 50, p. 21–29.

ZUFFA, G.G., 1985, Optical analyses of arenites: influence of methodology on compositional results, *in* Zuffa, G.G., ed., Provenance of Arenites: The Netherlands, Dordrecht, Reidel, p. 165–189.

ZUFFA, G.G., CIBIN, U., AND DI GIULIO, A., 1995, Arenite petrography in sequence stratigraphy: Journal of Geology, v. 103, p. 451–459.

ZUFFA, G.G., GAUDIO, W., AND ROVITO, S., 1980, Detrital mode evolution of the rifted continental-margin Longobucco sequence (Jurassic), Calabrian Arc, Italy: Journal of Sedimentary Petrology, v. 50, p. 51–61.